DNGR1-mediated Deletion of A20/Tnfaip3 in Dendritic Cells Alters T and B-cell Homeostasis and Promotes Autoimmune Liver Pathology

T. Das, I.M. Bergen, T. Koudstaal, J.A.C. van Hulst, G. van Loo, A. Boonstra, T. Vanwolleghem, P.S.C. Leung, M.E. Gershwin, R.W. Hendriks, M. Kool

Journal of Autoimmunity. 2019 Aug;102:167-178.

ABSTRACT

Dendritic cells (DCs) are central regulators of tolerance versus immunity. The outcome depends amongst others on DC subset and activation status. Whereas $CD11b^+$ type 2 conventional DCs (cDC2s) initiate proinflammatory helper T (Th)-cell responses, $CD103^+$ cDC1s are crucial for regulatory T-cell (Treg) induction and $CD8^+$ T-cell activation. DC activation is controlled by the transcription factor NF-κB. Ablation of A20/Tnfaip3, a critical regulator of NF-κB activation, in DCs leads to constitutive DC activation and development of systemic autoimmunity. We hypothesized that the activation status of cDCs controls the development of autoimmunity.

To target cDCs, DNGR1(*Clec9a)*-mediated excision of A20/Tnfaip3 was used through generation of *Tnfaip3*$^{fl/fl}$x*Clec9a*$^{+/cre}$ (*Tnfaip3*$^{DNGR1\text{-}KO}$) mice. Immune cell activation was evaluated at 31-weeks of age.

We found that DNGR1-mediated deletion of A20/Tnfaip3 resulted in liver pathology characterized by inflammatory infiltrates adjacent to the portal triads. Both cDC subsets as well as monocyte-derived DCs (moDCs) in *Tnfaip3*$^{DNGR1\text{-}KO}$ livers harbored an activated phenotype. Specifically, the costimulatory molecule CD40 in liver cDCs and moDCs was regulated by A20/Tnfaip3 expression. Livers from *Tnfaip3*$^{DNGR1\text{-}KO}$ mice had augmented proportions of Th1, Th17, Treg, and follicular Th (Tfh)-cells compared to control mice, accompanied by an increase in IgA-producing plasma cells. Serum IgA from *Tnfaip3*$^{DNGR1\text{-}KO}$ mice recognized self-proteins, specifically cytoplasmic proteins in liver periportal regions.

These data show that enhanced activation of cDCs and moDCs, due to A20/Tnfaip3 ablation, promotes the development of organ-specific autoimmunity but not systemic autoimmunity. This model could be useful to examine the pathobiological processes contributing to autoimmune liver diseases.

1. INTRODUCTION

The adaptive immune response is critically altered in autoimmune diseases, where activation of T-cells is induced by dendritic cells (DCs). DCs are also known as central regulators in the delicate balance between tolerance and immunity[1]. During steady state, immature DCs present self-antigens to T-cells, thereby inducing regulatory $CD4^+$ T-cell (Tregs), T-cell anergy or autoreactive T-cell deletion[2-4]. These mechanisms prevent T-cell mediated autoimmunity[5]. The balance between tolerance and immunity depends on the maturation status of DCs, a process that is strictly regulated[6, 7]. During infections and inflammation, DCs are activated through ligand-receptor interaction on DCs, which initiates the NF-κB pathway is initiated and provokes proinflammatory cytokine production[8]. NF-κB activation is tightly controlled by several mechanisms. One major inhibitor of NF-κB signalling is the ubiquitin-editing enzyme TNFα-induced protein 3 (TNFAIP3) or A20[9]. DC-specific deletion of *Tnfaip3*/A20 using the *Cd11c* promotor in mice (*Tnfaip3*$^{CD11c\text{-}KO}$ mice) resulted in spontaneous activation of DCs and induction of autoreactive $CD4^+$ T helper (Th)1-cells and Th17-cells differentiation, causing a severe and complex autoimmune inflammatory phenotype[10, 11]. *Tnfaip3*$^{CD11c\text{-}KO}$ mice developed features of inflammatory bowel disease[10] (IBD) and systemic lupus erythematosus (SLE)[11]. Importantly, genetic polymorphisms in the *TNFAIP3* gene are associated with several human autoimmune disorders[12, 13].

DCs comprise different subsets with specialized functions[5]. Both conventional DCs (cDCs) and plasmacytoid DCs (pDCs) are present during steady state. $CD103^+$/$CD8^+$ type 1 cDCs (cDC1s) are important for peripheral tolerance as they can present tissue-associated self-antigens[5]. During steady state, cDC1s can induce Tregs[14-16], Th-cell deletion[17], $CD8^+$ T-cell tolerance[17, 18], and once activated, cDC1s also provoke cytotoxic T-cell responses[19]. Strikingly, ablation of cDC1s does not cause spontaneous autoimmunity[19, 20], it only alters intestinal T-cell homeostasis[21]. Under steady state, $CD11b^+$/$CD4^+$ type 2 cDCs (cDC2s) also induce T-cell tolerance[22], and provoke Treg proliferation and differentiation[16, 23]. Activated cDC2s strongly promote Th-cell activation and induce Th-cell differentiation into Th2[24] or Th17-cells[25]. During inflammation, monocyte-derived DCs (moDCs) arise and produce chemokines to attract immune cells to the inflammatory lesion[26].

It is unclear what the contribution of different DC subsets is to the autoimmune phenotype in *Tnfaip3*$^{CD11c\text{-}KO}$ mice. As cDCs are important instructors of T-cell tolerance, we hypothesized that cDCs crucially contribute to the autoimmune phenotype. To determine cDC function, we used DNGR1-driven[27] deletion of *Tnfaip3*/A20 (*Tnfaip3*$^{DNGR1\text{-}KO}$ mice) as DNGR1-driven cre-expression can induce efficient deletion of target genes in ~95% of organ cDC1s, 25-40% of cDC2s, and ~5-25% of moDCs in wildtype mice [27].

2. MATERIAL & METHODS

2.1. Mice

Male and female mice harbouring a conditional *Tnfaip3* allele flanked by LoxP sites[28] were crossed to mice expressing the Cre recombinase under the *Clec9a* promotor (DNGR1)[27], generating *Tnfaip3*$^{fl/fl}$x*Clec9a*$^{+/cre}$ mice (*Tnfaip3*$^{DNGR1\text{-}KO}$ mice). Mice were >10 times back-crossed to obtain a C57Bl/6 background. *Tnfaip3*$^{fl/fl}$x*Clec9a*$^{+/+}$ littermates (*Tnfaip3*$^{DNGR1\text{-}WT}$ mice) served as controls. All mice were sacrificed between 11-31 weeks of age.

To trace Tnfaip3-deletion and function in cDCs, we crossed *Tnfaip3*$^{+/+}$x*Clec9a*$^{+/cre}$ mice to Rosa26-Stop$^{fl/fl}$-YFP mice[29] (*Tnfaip3*$^{DNGR1\text{-}ROSA\text{-}WT}$ mice) and *Tnfaip3*$^{fl/fl}$x*Clec9a*$^{+/cre}$ mice to Rosa26-Stop$^{fl/fl}$-YFP mice (*Tnfaip3*$^{DNGR1\text{-}ROSA\text{-}KO}$ mice). Mice were housed under specific pathogen-free conditions and had ad libitum access to food and water. All experiments were approved by the animal ethical committee of the Erasmus MC, Rotterdam, The Netherlands and comply to the EU Directive 2010/63/EU for animal experiments.

2.2. Cell suspension preparation

Spleen and liver were isolated and used for flow cytometry. Spleens were homogenized through a 100-µm cell strainer. Erythroid cells present in the spleen cell suspensions were lysed using osmotic lysis buffer (8.3% NH_4CL, 1% $KHCO_3$, and 0.04% NA_2EDTA in Milli-Q). Liver single-cell suspensions were obtained, as previously described[30], by digesting with Liberase TM (Roche, Basel, Switzerland) for 30 minutes at 37°C. After digestion, the livers were homogenized using a 100-µm cell strainer (Fischer Scientific). Hepatocytes were discarded using two low speed centrifuge steps. Lastly, erythroid cells were lysed using osmotic lysis buffer.

2.3. Flow cytometry procedures

Flow cytometry surface and intracellular staining procedures have been described previously[31]. Monoclonal antibodies used for flow cytometric analyses are listed in **Supplementary table 1**. For all experiments, dead cells were excluded using fixable Amcyan viability dye (eBioscience, San Diego, CA, USA). To measure cytokine production, cells were stimulated with 10 ng/mL PMA (Sigma-Aldrich, St. Louis, MI, USA) and 250 ng/mL ionomycin (Sigma-Aldrich) in the presence of GolgiStop (BD Biosciences, San Jose, CA, USA) for 4 h at 37°C. Flow cytometry absolute counting beads (Polysciences, Warrington, PA, USA) were added to liver flow cytometry samples. Data were acquired using an LSR II flow cytometer (BD Biosciences) with FACS Diva™ software and analyzed by FlowJo version 9 (Tree Star Inc software, Ashland, OR, USA).

2.4. Liver histology

The right lobe of the liver was fixated with 4% PFA (Carl Roth, Karlsruhe, Germany) for 24 hr before paraffin embedding. Six-µm-thick paraffin embedded liver sections were stained with hematoxylin and eosin, and using Sirius Red (Sigma-Aldrich) and Fast Green (Sigma-Aldrich) to stain for collagen fibers, as previously described[32]. Liver pathology was scored using the histopathologic scoring system according to Ishak et al.[33] For immunohistochemical stainings, antigen retrieval on paraffin-sections was established using citrate buffer (Sigma-Aldrich).

Paraffin sections were stained for Cytokeratin 7, CD3 and B220. The primary antibodies used for immunohistochemistry are listed in **Supplementary table 2**. Sections were incubated for 1 hr with the primary antibodies. After washing, slides were incubated for 30 minutes with secondary antibodies (**Supplementary table 2**). On paraffin sections which were stained for Cytokeratin 7 and CD3, the anti-Rabbit ABC Peroxidase Kit was utilized (Vector Labs, Burlingame, CA, USA). Diaminobenzene (DAB) and Fast Blue Alkaline phosphatase substrates were used to retrieve specific staining.

2.5. Serum measurements

To determine liver function, aspartate aminotransferase (AST) and alanine aminotransferase (ALT) enzymes were measured in serum.

For total immunoglobulin concentrations, Nunc Microwell plates (Life technologies, Carlsbad, CA, USA) were coated with 1 µg/ml goat-anti-mouse IgM, IgA, IgG1, IgG2a, IgG2b, or IgG3 (Southern Biotech, Birmingham, AL, USA) overnight at 4C°. Wells were blocked with 10% FCS (Capricorn Scientific, Ebsdorfergrund, Germany) in PBS (Thermo Scientific, Waltham, MA, USA) for 1 hr. Standards and serum were diluted in PBS and incubated for 3 hrs at room temperature. Depending on the isotype of interest, anti-mouse biotin-labeled IgM, IgA, IgG1, IgG2a, IgG2b, or IgG3 (Southern Biotech) was incubated for 1 hr. Streptavidin-HRP (eBioscience) and TMB substrate (eBioscience) was used to develop the ELISA and then optical density (OD) was measured at 450 nm on a Microplate Reader (Bio-Rad, Hercules, CA, USA).

For detection of anti-cardiolipin antibodies, Nunc Microwell plates were coated with 10 µg/ml cardiolipin from bovine heart (Sigma) in ethanol and left to dry overnight. For detection of dsDNA, 20µg/ml dsDNA from calf thymus (Sigma) was coated overnight on pre-coated poly-l-lysine microwells. Wells were blocked with 2% BSA/PBS for 2 hrs, after which serum was incubated for 2 hrs. Anti-mouse IgG1 biotin/streptavidin-HRP (eBioscience) was used to develop the ELISA with TMB substrate (eBioscience). Detection of immunoglobulin IgG/IgA versus PDC-E2, sp100 and gp210 was performed as previously described[34].

For detection of autoreactive IgA binding to tissues, we used 5µm cryo-sectioned liver and pancreas from $Rag1^{KO}$ mouse[35], as these mice lack mature B-cells and conse-

quently endogenous immunoglobulins are absent. After 10 minutes acetone fixation (Sigma) and 10 minutes block with 10% normal goat serum (NGS), sera from *Tnfaip3*$^{DNGR1\text{-}WT}$ mice (dilution 1/33) and *Tnfaip3*$^{DNGR1\text{-}KO}$ mice (dilution 1/100) were incubated for 1 hr. Different dilutions were used to correct for total IgA concentrations in serum from *Tnfaip3*$^{DNGR1\text{-}WT}$ and *Tnfaip3*$^{DNGR1\text{-}KO}$ mice. Incubation with anti-mouse IgA biotin/streptavidin (BD) and subsequently goat anti-Rat-AP (Sigma), followed by New Fuchsine (Sigma) staining were used to visualize liver-specific IgA. Slides were counterstained with Gills hematoxylin (Sigma).

2.6. Statistics

Statistical significance of data was calculated using the non-parametric Mann Whitney U test. P-values <0.05 were considered significant. All analyses were performed using Prism (GraphPad Software version 9, La Jolla, CA, USA). All data are presented as the mean with the standard error of the mean (SEM).

3. RESULTS

3.1. *Tnfaip3*$^{DNGR1\text{-}KO}$ mice have spontaneous periportal liver infiltrates and signs of chronic inflammation.

To investigate whether immune homeostasis is altered when cDCs harbor a DNGR1-mediated deletion of the A20/*Tnfaip3* gene, we evaluated 31-week-old *Tnfaip3*^{DNGR1} mice. *Tnfaip3*$^{DNGR1\text{-}KO}$ mice had splenomegaly and hyper cellularity in contrast to *Tnfaip3*$^{DNGR1\text{-}WT}$ littermate controls (**Supplementary Figure 1A**). Splenic DC and T-cell numbers did not differ between *Tnfaip3*$^{DNGR1\text{-}KO}$ mice and *Tnfaip3*$^{DNGR1\text{-}WT}$ mice (**Supplementary Figure 1B-C**). Mainly marginal zone B-cells contributed to the increase of total splenic B-cells numbers in *Tnfaip3*$^{DNGR1\text{-}KO}$ mice compared to *Tnfaip3*$^{DNGR1\text{-}WT}$ mice (**Supplementary Figure 1D**).

We next evaluated kidneys, pancreas, intestines, and livers in 31-week-old *Tnfaip3*$^{DNGR1\text{-}KO}$ mice for signs of inflammation. Spleens of *Tnfaip3*$^{DNGR1\text{-}KO}$ mice showed mild architectural changes of the white pulp lymphoid follicles in comparison to WT mice (**Supplementary Figure 2A**). Pancreas, terminal ileum, colon, and kidneys of *Tnfaip3*$^{DNGR1\text{-}KO}$ mice did not show any sign of inflammation or remodelling (**Supplementary Figure 2B-E**). In contrast, livers of all *Tnfaip3*$^{DNGR1\text{-}KO}$ mice showed periportal inflammatory infiltrates at 31-weeks of age compared to WT mice (**Figure 1A/B**). Mild interface hepatitis (also known as piecemeal necrosis) and focal necrosis with inflammation, that are often seen in autoimmune hepatitis (AIH)[36], could also be observed *Tnfaip3*$^{DNGR1\text{-}KO}$ mice, but not in WT mice (**Figure 1C/D**). Mild liver fibrosis also occurred around portal triads of *Tnfaip3*$^{DNGR1\text{-}KO}$ mice compared to controls (**Figure 1E/F**). These features resulted in

a significantly higher liver histopathologic score for *Tnfaip3*$^{DNGR1\text{-}KO}$ mice compared to WT mice (**Figure 1G**). Also increased cytokeratin 7 expression, a protein expressed in bile ducts and indicative for ductular reaction, could be observed in *Tnfaip3*$^{DNGR1\text{-}KO}$ mice compared to littermate controls (**Figure 1H**). Furthermore, a mild, but significant, in-

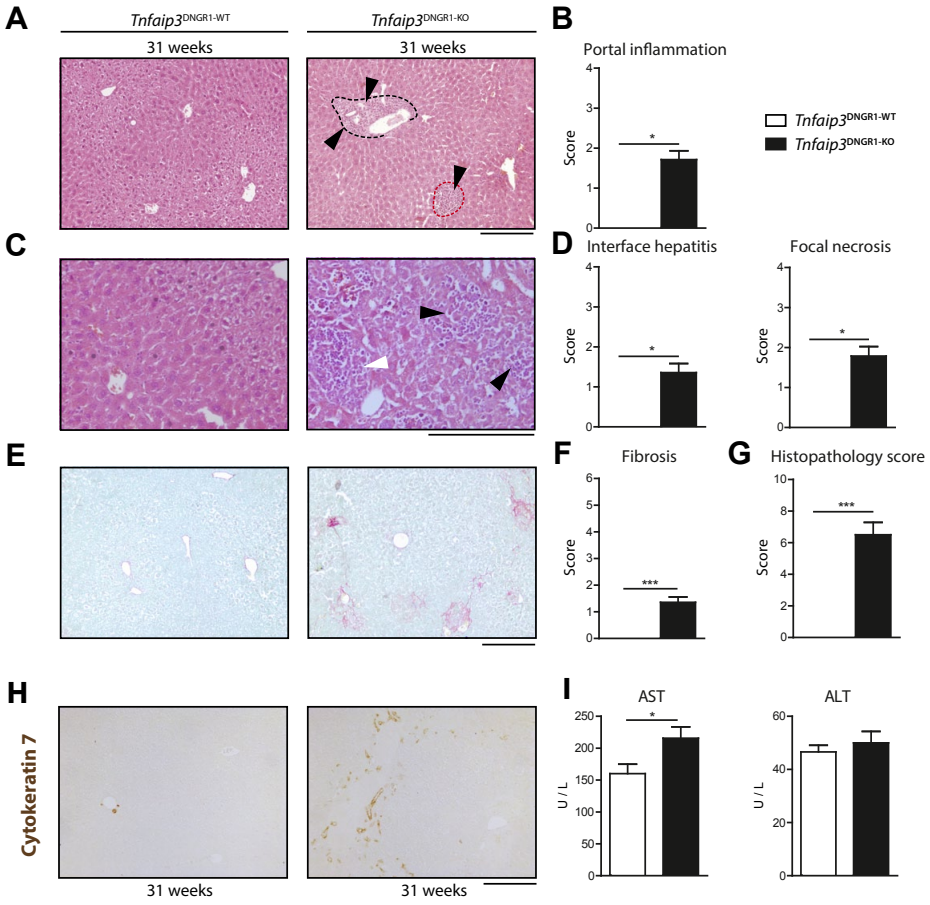

Figure 1: *Tnfaip3*$^{DNGR1\text{-}KO}$ mice have spontaneous periportal liver infiltrates and signs of chronic inflammation.

Tnfaip3$^{DNGR1\text{-}WT}$ mice and *Tnfaip3*$^{DNGR1\text{-}KO}$ mice were analyzed at 31-weeks of age. (A) Hematoxylin and eosin (H&E) stained liver histology with periportal infiltrates (black dashed line) and lobular infiltrates (red dashed line). (B) Quantification of the portal inflammation score (max. 4). (C) Larger magnification H&E stained liver histology indicating areas of interface hepatitis (white arrow) and focal necrosis with inflammation (black arrows). (D) Quantified interface hepatitis and focal necrosis with inflammation score (max. 4). (E-F) Sirius Red staining to stain collagen fibers (E) and enumeration of the resulting fibrosis score (max. 6) (F). (G) Quantification of the total histopathology score (max. 18). (H) Immunohistochemistry of livers for Cytokeratin 7 (brown). (I) Quantification of serum liver enzymes AST and ALT in 31-week-old *Tnfaip3*$^{DNGR1\text{-}WT}$ mice and *Tnfaip3*$^{DNGR1\text{-}KO}$ mice. Scale bars represent 200 µm. Results of pooled data from 3 experiments and are presented as mean ± SEM of $n = 15$ mice per group. $^{*}P < 0.05$, $^{***}P < 0.001$.

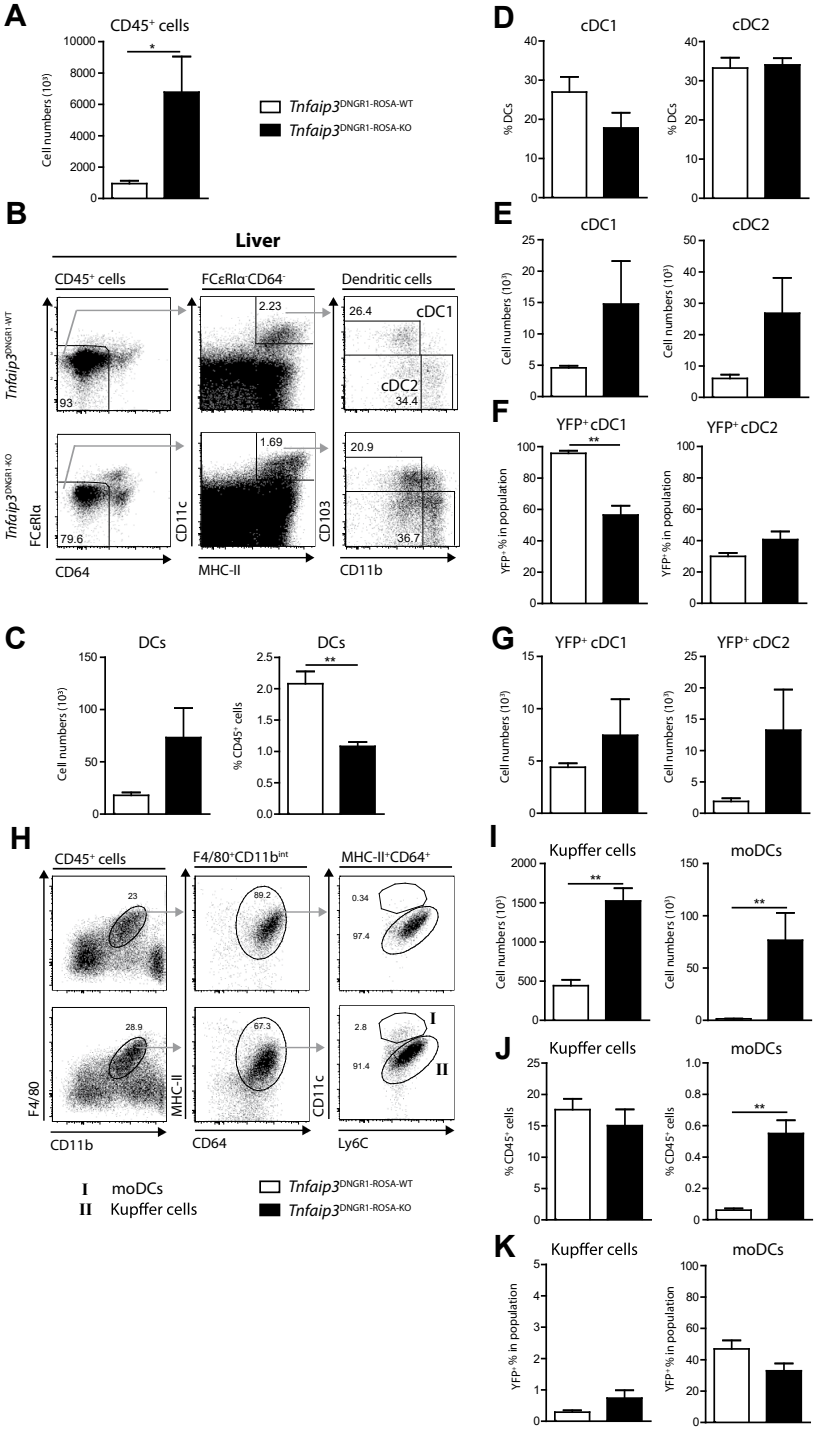

Figure 2: DNGR1-mediated deletion of A20/*Tnfaip3* targets both cDCs and mo-DCs

Tnfaip3$^{DNGR1\text{-}ROSA\text{-}WT}$ mice and *Tnfaip3*$^{DNGR1\text{-}ROSA\text{-}KO}$ mice were analyzed at 31-weeks of age. (A) Enumeration of liver CD45$^+$ cells. (B) Flow cytometric gating strategy of liver cDC1s (CD103$^+$ CD11b$^-$CD11c^{hi}MHC-II^{hi}FcεRIα$^-$CD64$^-$) and cDC2s (CD11b$^+$CD103$^-$CD11c^{hi}MHC-II^{hi}FcεRIα$^-$CD64$^-$). Representative flow cytometry examples are shown from *Tnfaip3*$^{DNGR1\text{-}ROSA\text{-}WT}$ mice and *Tnfaip3*$^{DNGR1\text{-}ROSA\text{-}KO}$ mice. (C) Total DC number and proportion of CD45$^+$ cells. (D-G) Quantification of cDC1s and cDC2s as a proportion of liver DCs (D), cell numbers (E), proportion of YFP$^+$ expressing cells (F) and the YFP$^+$ cell numbers (G). (H) Flow cytometric gating strategy of liver Kupffer cells (F4/80$^+$CD11b^{int}MHC-II^{hi}CD64$^+$CD11c$^{lo/int}$) and moDCs (F4/80$^+$CD11b^{int}MHC-II^{hi}CD64$^+$CD11c^{hi}) in *Tnfaip3*$^{DNGR1\text{-}WT}$ mice and *Tnfaip3*$^{DNGR1\text{-}KO}$ mice. (I-K) Quantification of Kupffer cell and moDC numbers (I), proportion of CD45$^+$ hematopoietic cells (J), and proportion of YFP$^+$ expressing cells (K) using flow cytometry. Representative data is shown from one experiment of 2 independent experiments. Results are presented as mean ± SEM of n = 4-7 mice per group. *P<0.05, **P<0.01.

crease in serum aspartate aminotransferase (AST) was observed in *Tnfaip3*$^{DNGR1\text{-}KO}$ mice compared to WT controls (**Figure 1I**). No differences were observed between male or female *Tnfaip3*$^{DNGR1\text{-}KO}$ mice (data not shown).

Summarizing, these data illustrate that aged *Tnfaip3*$^{DNGR1\text{-}KO}$ mice develop a spontaneous liver pathology characterized by the presence of periportal inflammatory infiltrates and signs of chronic inflammation.

3.2. DNGR1-mediated deletion of A20/*Tnfaip3* targets both cDCs and mo-DCs.

In line with histological findings, the total number of liver CD45$^+$ hematopoietic cells was increased in *Tnfaip3*$^{DNGR1\text{-}ROSA\text{-}KO}$ mice compared to *Tnfaip3*$^{DNGR1\text{-}ROSA\text{-}WT}$ mice (**Figure 2A**). Within liver CD45$^+$ cells, we determined the different DC subsets (**Figure 2B**). The proportion of DCs from total CD45$^+$ cells was lower in *Tnfaip3*$^{DNGR1\text{-}ROSA\text{-}KO}$ mice compared to *Tnfaip3*$^{DNGR1\text{-}ROSA\text{-}WT}$ mice, but total liver DC numbers were not significantly different (**Figure 2C**). Conventional DC1s and cDC2s were neither significantly altered as proportions of DCs nor in cell numbers between the two genotypes (**Figure 2D/E**). To investigate DNGR1-cre mediated deletion efficiency and the effect of A20/Tnfaip3 ablation on liver cDC homeostasis, we examined *Tnfaip3*$^{DNGR1\text{-}ROSA\text{-}WT}$ mice and *Tnfaip3*$^{DNGR1\text{-}ROSA\text{-}KO}$ mice, in which YFP expression can be used as a lineage tracer of DNGR1 expression. DNGR1-lineage tracing studies revealed that DNGR1-mediated cre-recombinase activity targeted almost all mature cDC1s and ~30% of cDC2s. As mature cDC2s do not express DNGR1[27], this ~30% deletion is caused by DNGR1-cre efficacy in cDC progenitors, which do express DNGR1 although to a lower extent[27]. Similar to other organs[27], in livers of *Tnfaip3*$^{DNGR1\text{-}ROSA\text{-}WT}$ mice ~95% of cDC1s showed YFP expression, which was reduced to ~55% in *Tnfaip3*$^{DNGR1\text{-}ROSA\text{-}KO}$ mice (**Figure 2F**). YFP expression in liver cDC2s did not differ between *Tnfaip3*$^{DNGR1\text{-}ROSA\text{-}WT}$ mice and *Tnfaip3*$^{DNGR1\text{-}ROSA\text{-}KO}$ mice and remained ~35% (**Figure 2F**). The absolute number of YFP$^+$ cDC1s was similar between *Tnfaip3*$^{DNGR1\text{-}ROSA\text{-}WT}$ mice and *Tnfaip3*$^{DNGR1\text{-}ROSA\text{-}KO}$ mice (**Figure 2G**). Plasmacytoid DCs in liver were unaffected by DNGR1-mediated deletion (~2% YFP$^+$; data not shown). We next determined Kupffer cells and monocyte-derived DCs (moDCs) (**Figure 2H**). The total number of both Kupffer

cells and moDCs was increased in *Tnfaip3*$^{DNGR1\text{-}KO}$ mice compared to *Tnfaip3*$^{DNGR1\text{-}WT}$ mice (**Figure 2I**). While Kupffer cell proportions of CD45^{+} cells were similar, moDCs significantly expanded as a proportion of CD45^{+} cells in *Tnfaip3*$^{DNGR1\text{-}KO}$ mice compared to littermate controls (**Figure 2J**). YFP expression was almost absent in Kupffer cells (<1%) in both genotypes (**Figure 2K**). Liver moDCs, albeit present in low numbers in *Tnfaip3*$^{DNGR1\text{-}ROSA\text{-}WT}$ mice, harbored a slightly higher YFP expression WT mice (~45%) compared to and in *Tnfaip3*$^{DNGR1\text{-}ROSA\text{-}WT}$ and *Tnfaip3*$^{DNGR1\text{-}ROSA\text{-}KO}$ mice (~30%) (**Figure 2K**).

Concluding, DNGR1-lineage tracing indicated that in livers of control mice respectively 95% and 35% of cDC1s and cDC2s, as well as 45% of moDCs express or once expressed DNGR1. Furthermore, due to deletion of A20/Tnfaip3 55% and 35% of liver cDC1s and cDC2s, along with 30% of liver moDCs were affected by DNGR1-targeting.

3.3. Surface CD40 expression is increased through both cell-intrinsic and cell-extrinsic effects of Tnfaip3-deficiency in cDC1s, cDC2s, and moDCs.

In livers of *Tnfaip3*$^{DNGR1\text{-}KO}$ mice, both cDC1s and cDC2s showed significantly enhanced surface expression of the costimulatory molecule CD40 compared to *Tnfaip3*$^{DNGR1\text{-}WT}$ mice (**Figure 3A/B**). In *Tnfaip3*$^{DNGR1\text{-}WT}$ mice, expression of the co-inhibitory molecule PD-L1 was higher in cDC2s than in cDC1s (**Figure 3B**). Both cDC1s and cDC2s in *Tnfaip3*$^{DNGR1\text{-}KO}$ mice significantly increased PD-L1 expression in comparison to *Tnfaip3*$^{DNGR1\text{-}WT}$ mice (**Figure 3A/B**). No differences were observed for MHC-I or MHC-II expression in cDCs (data not shown).

We next analyzed whether the altered co-stimulatory molecule expression was a direct consequence of A20/Tnfaip3-deletion, and compared YFP^{+} and YFP^{-} cDCs, indicative of A20/Tnfaip3-deficient or A20/Tnfaip3-sufficient cDCs respectively in Tnfaip3$^{DNGR1\text{-}ROSA\text{-}KO}$ mice. YFP^{+} cDC1s and YFP^{+} cDC2s from *Tnfaip3*$^{DNGR1\text{-}ROSA\text{-}KO}$ mice harboured significantly higher CD40 expression in comparison to YFP^{-} cDCs within the same livers (**Figure 3C**), whereas PD-L1 expression was similar in YFP^{+} and YFP^{-} cDC1s/cDC2s from *Tnfaip3*$^{DNGR1\text{-}ROSA\text{-}KO}$ mice (**Figure 3D**). CD40 and PD-L1 expression was already enhanced on YFP-negative Tnfaip3-sufficient cDC1s/cDC2s from *Tnfaip3*$^{DNGR1\text{-}ROSA\text{-}KO}$ mice compared to Tnfaip3-sufficient cDC1s/cDC2s in *Tnfaip3*$^{DNGR1\text{-}ROSA\text{-}WT}$ mice (**Figure 3C/D**). CD40 expression on liver moDCs did not differ between *Tnfaip3*$^{DNGR1\text{-}KO}$ mice and WT controls (**Figure 3E/F**). In contrast, YFP^{+} moDCs of *Tnfaip3*$^{DNGR1\text{-}ROSA\text{-}KO}$ mice showed a higher CD40 expression than YFP^{-} moDCs (**Figure 3G/H**). Liver moDCs also harboured higher PD-L1 expression in *Tnfaip3*$^{DNGR1\text{-}KO}$ mice compared to *Tnfaip3*$^{DNGR1\text{-}WT}$ controls (**Figure 3E/F**), but this did not differ between YFP^{+} or YFP^{-} moDCs in *Tnfaip3*$^{DNGR1\text{-}ROSA\text{-}KO}$ mice (**Figure 3G/H**).

In summary, both liver cDC1s and cDC2s of *Tnfaip3*$^{DNGR1\text{-}KO}$ mice show an activated phenotype, e.g. increased CD40 and PD-L1 expression, irrespective of Tnfaip3 deletion. Only CD40 expression is specifically enhanced due to cell-intrinsic loss of Tnfaip3. Liver moDCs of *Tnfaip3*$^{DNGR1\text{-}KO}$ mice show elevated PD-L1 expression compared to

Tnfaip3$^{DNGR1\text{-}WT}$ mice. Strikingly, enhanced CD40 expression is specifically observed in *Tnfaip3*-deficient moDCs.

3.4. Livers of *Tnfaip3*$^{DNGR1\text{-}KO}$ mice have increased proportions of Th1-cells, Th17-cells and Tregs.

The proportion of CD8$^+$ T-cells and natural killer (NK)-cells within CD45$^+$ cells were elevated in the livers of *Tnfaip3*$^{DNGR1\text{-}KO}$ mice compared to control mice (**Figure 4A**). The percentage of CD4$^+$ Th-cells and neutrophils were reduced in *Tnfaip3*$^{DNGR1\text{-}KO}$ mice compared to *Tnfaip3*$^{DNGR1\text{-}WT}$ controls (**Figure 4A**). Liver F4/80$^+$ macrophages and Kupffer cells, monocytes, and B-cell percentages were not significantly different (**Figure 4A**). Due to an increase in absolute numbers of CD45$^+$ hematopoietic cells (**Figure 2A**), the total number of CD8$^+$ T-cells, CD4$^+$ Th-cells, and B-cells were significantly increased in *Tnfaip3*$^{DNGR1\text{-}KO}$ mice compared to controls (**Figure 4B**). Clusters of T-cells and B-cells were observed in the periportal infiltrates of *Tnfaip3*$^{DNGR1\text{-}KO}$ mice, while only occasionally among hepatocytes in *Tnfaip3*$^{DNGR1\text{-}WT}$ mice (**Figure 4C**). In *Tnfaip3*$^{DNGR1\text{-}KO}$ mice, the majority of inflammatory lesions in the portal triads consisted of T-cells only (**Figure 4C**). In addition, clusters of DCs and CD8$^+$ T-cells were localised in periportal infiltrates in *Tnfaip3*$^{DNGR1\text{-}KO}$ mice, compared to sparsely located DCs and CD8$^+$ T-cells in control mice (**Supplementary Figure 3A**). DNGR1$^+$ cells, most likely cDC1s, were also localised within these periportal infiltrates of *Tnfaip3*$^{DNGR1\text{-}KO}$ mice (**Supplementary Figure 3B**).

The percentage of effector CD44$^+$ CD8$^+$ T-cells was increased in *Tnfaip3*$^{DNGR1\text{-}KO}$ mice compared to WT controls, however the percentage of granzyme B or interferon gamma (IFNγ)-positive CD8$^+$ T-cells was unaltered (**Supplementary Figure 4**). No differences were observed in the proportions of CD44$^+$ effector liver Th-cells (**Figure 4D**), but the proportions of liver Foxp3$^+$CD25$^+$ Tregs were augmented in *Tnfaip3*$^{DNGR1\text{-}KO}$ mice in comparison to WT mice (**Figure 4E**). Increased percentages of IFNγ single-positive, IFNγ/IL-10 double-producing, and IL-17A single-positive Th-cells were found in livers of *Tnfaip3*$^{DNGR1\text{-}KO}$ mice compared to WT mice (**Figure 4F/G/H**). No differences were observed in IL-10 single-positive Th-cells (**Figure 4G**). Interleukin-12-positive cells could also be observed within the periportal infiltrates in *Tnfaip3*$^{DNGR1\text{-}KO}$ mice (**Supplementary Figure 3C**).

In summary, liver CD8$^+$ T-cells, Th-cells, and B-cells in *Tnfaip3*$^{DNGR1\text{-}KO}$ mice increase in number due to a total increase in hematopoietic cells and they accumulate in the periportal regions. Th-cells within livers from *Tnfaip3*$^{DNGR1\text{-}KO}$ mice showed augmented proportions of IFNγ and IL-17A single-producing Th-cells and IFNγ/IL-10 double-producing Th-cells.

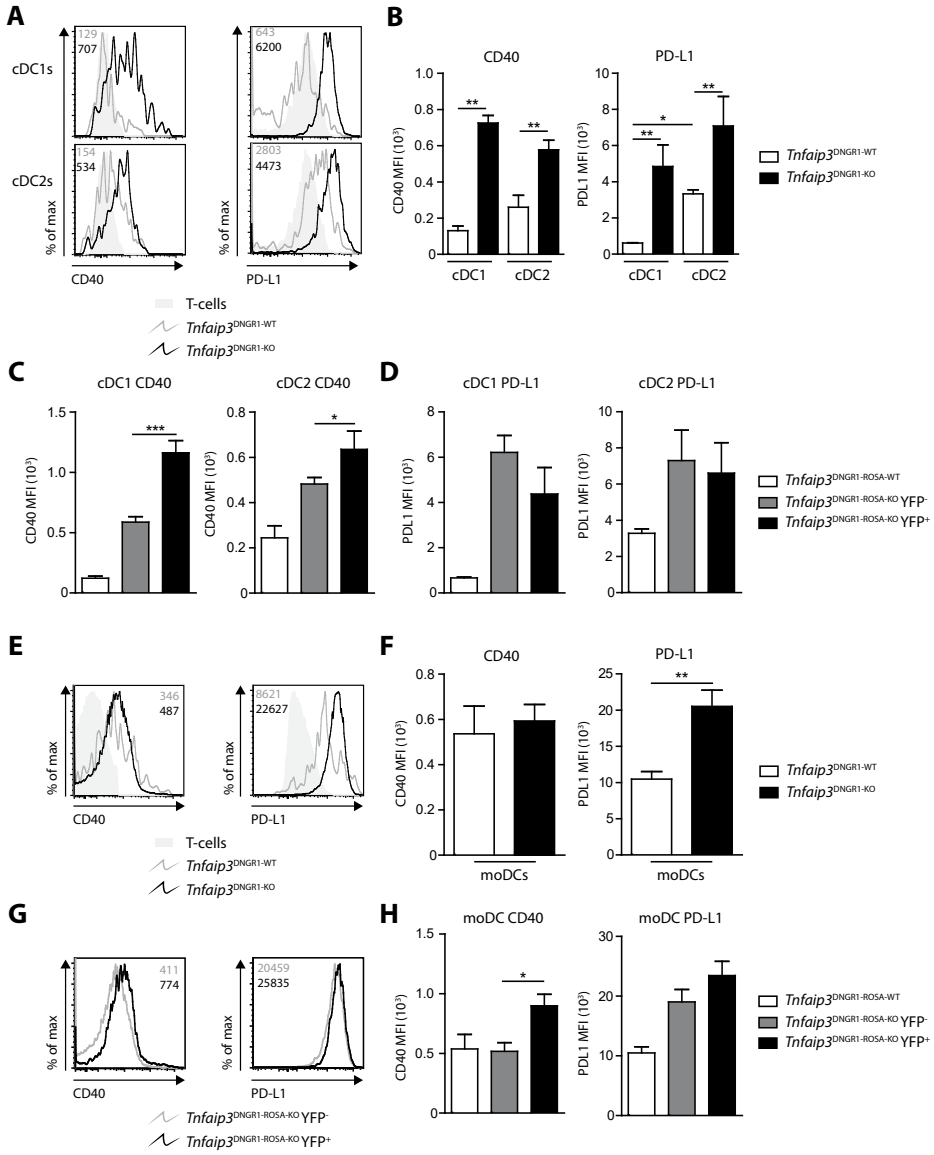

Figure 3: CD40 expression is increased through both cell-intrinsic and cell-extrinsic effects of Tnfaip3-deficiency in cDC1s, cDC2s, and moDCs.

Tnfaip3$^{DNGR1\text{-}ROSA\text{-}WT}$ mice and *Tnfaip3*$^{DNGR1\text{-}ROSA\text{-}KO}$ mice were sacrificed at 31-weeks of age. (A) Histograms showing expression of CD40 and PD-L1 on liver cDC1s and cDC2s. (B) Quantification of CD40 and PD-L1 by median fluorescence intensity (MFI) on liver cDC1s and cDC2s. (C-D) Quantification of CD40 MFI (C) and PD-L1 MFI (D) in YFP-positive and YFP-negative liver cDC1s and cDC2s. (E) Histograms showing expression of CD40 and PD-L1 on liver moDCs. (F) Quantification of CD40 and PD-L1 by MFI on liver moDCs. (G) Histograms illustrating expression of CD40 and PD-L1 on liver YFP$^+$ and YFP$^-$ moDCs in *Tnfaip3*$^{DNGR1\text{-}ROSA\text{-}KO}$ mice. (H) Quantification of CD40 and PD-L1 by MFI in YFP-positive and YFP-negative liver moDCs in *Tnfaip3*$^{DNGR1\text{-}ROSA\text{-}KO}$ mice. Representative data is shown from one experiment of 2 independent experiments.

Results are presented as mean ± SEM of n = 4-7 mice per group. Significance in (C,H) is only shown for YFP$^+$ and YFP$^-$ cells in *Tnfaip3*$^{DNGR1\text{-}ROSA\text{-}KO}$ mice. *P < 0.05, **P<0.01.

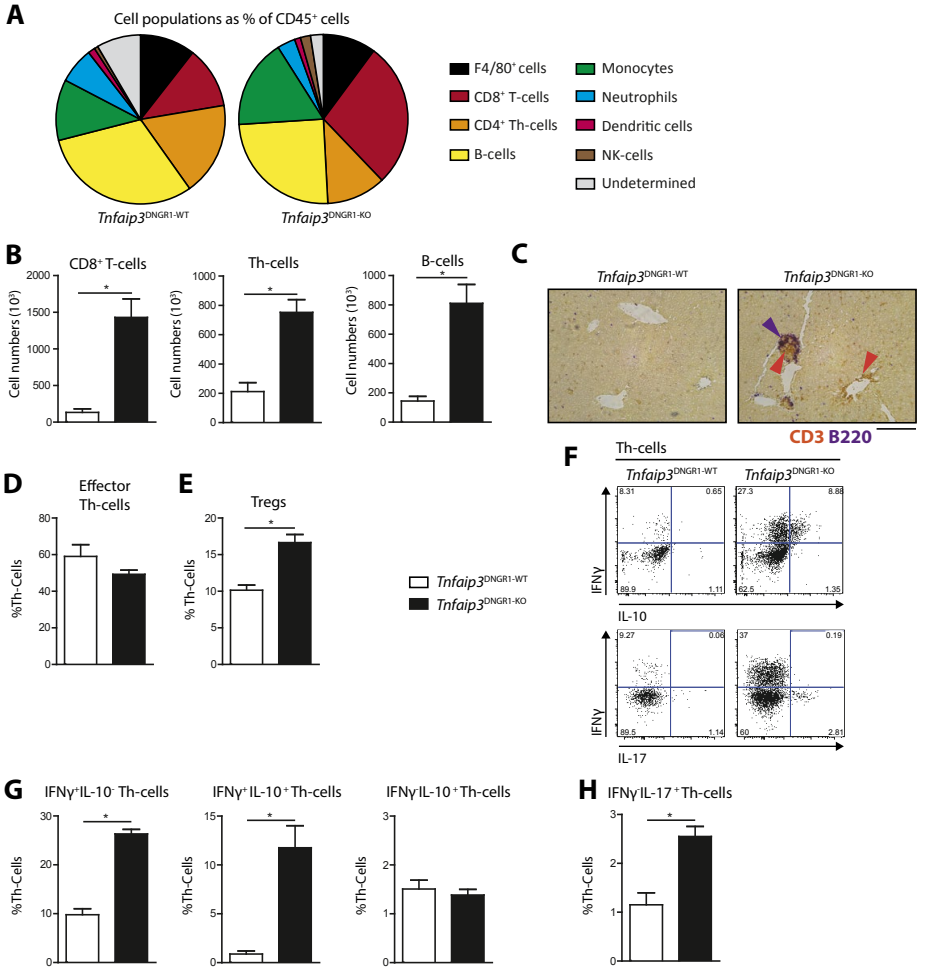

Figure 4: Livers of *Tnfaip3*$^{DNGR1\text{-}KO}$ mice have increased proportions of Th1-cells, Th17-cells and Tregs. *Tnfaip3*$^{DNGR1\text{-}WT}$ mice and *Tnfaip3*$^{DNGR1\text{-}KO}$ mice were sacrificed at 31-weeks of age. (A) Representation of liver immune cell proportions, being F4/80$^+$ cells (CD45$^+$F4/80$^+$CD11b^{int}), CD8$^+$ T-cells (CD3$^+$CD8$^+$), Th-cells (CD3$^+$CD4$^+$), B-cells (CD19$^+$), monocytes (CD11b$^+$CD11c$^-$GR1$^-$NK1.1$^-$), neutrophils (CD11b$^+$GR1$^+$NK1.1$^-$), total DCs, and NK-cells (NK1.1$^+$, GR1$^-$). (B) Quantification of CD8$^+$ T-cells, Th-cells and B-cells (CD19$^+$B220$^+$) in liver. (C) Immunohistochemistry of livers for CD3$^+$ (brown, T-cells) and B220$^+$ (purple, B-cells) cells in 31-week-old *Tnfaip3*$^{DNGR1\text{-}KO}$ mice and *Tnfaip3*$^{DNGR1\text{-}WT}$ mice also indicated by arrowheads. (D-E) Quantification of the proportion activated (CD44$^+$) Th-cells (D) and Tregs (E) using flow cytometry. (F) A representative example of flow cytometry data of liver CD4$^+$ Th-cells with IFNγ, IL-10 and IL-17A production is shown for *Tnfaip3*$^{DNGR1\text{-}WT}$ mice and *Tnfaip3*$^{DNGR1\text{-}KO}$ mice. (G-H) Percentages of cytokine-producing Th-cells is shown, being IFNγ single-positive, IFNγ/IL-10 double-positive, IL-10 single-positive (G) and IL-17A single-positive (H) using flow cytometry. Representative data from one experiment is shown out of 4 experiments for (B, D), 2 experiments (G-H) or 1 experiment (A,C). Results are presented as mean ± SEM of n =4 mice per group. *P < 0.05.

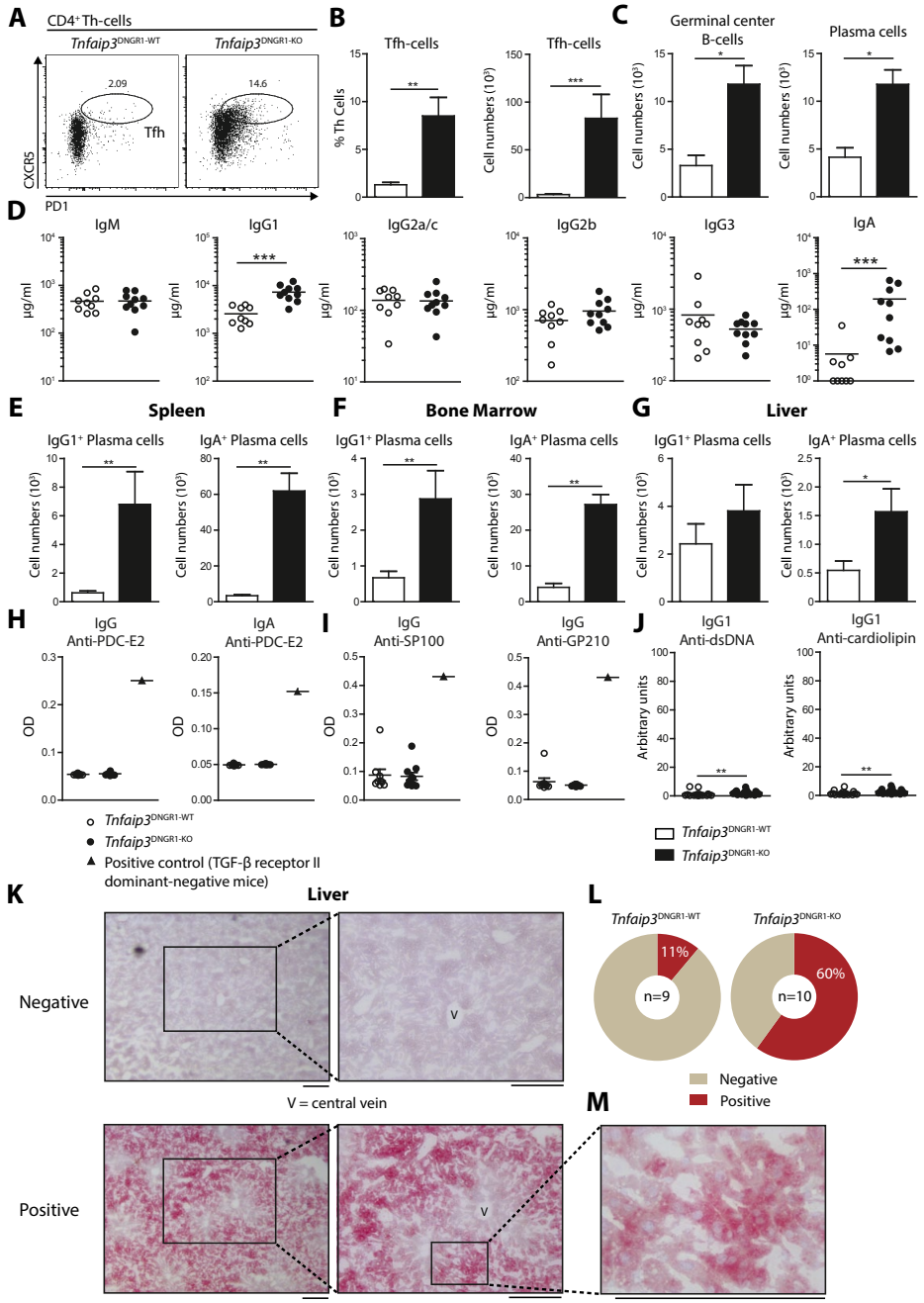

Figure 5: Livers of *Tnfaip3*$^{DNGR1-KO}$ mice contain increased Tfh-cells and plasma cells, likely producing liver-specific IgA antibodies.

Tnfaip3$^{DNGR1-WT}$ mice and *Tnfaip3*$^{DNGR1-KO}$ mice were sacrificed at 31-weeks of age. (A) Flow cytometry data of liver Tfh-cells ($CD3^+CD4^+CXCR5^+PD1^+$) from *Tnfaip3*$^{DNGR1-KO}$ mice and control mice. (B) Quantification of

the proportion Tfh-cells and cell numbers. (C) Enumeration of liver GC B-cells ($CD19^+B220^+CD95^+IgD^-$) and plasma cells ($B220^-CD138^+$). (D) Quantification of all serum immunoglobulin isotypes in 31-week-old mice. (E-G) Enumeration of $IgG1^+$ plasma cells ($B220^-CD138^+IgG1^+$) and IgA^+ plasma cells ($B220^-CD138^+IgGA^+$) in spleen (E), bone marrow (F), and liver (G). (H-J) Assessment of autoreactive IgG and IgA immunoglobulins towards PDC-E2 (H), IgG towards sp100 and gp210 (I) and IgG1 towards dsDNA and cardiolipin (J) in serum from 31-week-old mice using ELISA. 100 arbitrary units represent the average level of lupus-prone *lpr* mice in (J). (K) Livers from *Rag1*^{KO} mice were incubated with serum from 31-week-old *Tnfaip3*$^{DNGR1\text{-}WT}$ and *Tnfaip3*$^{DNGR1\text{-}KO}$ mice and assessed for IgA binding. (L) Negative and positive autoreactive IgA staining numbers on *Rag1*^{KO} livers using serum from *Tnfaip3*$^{DNGR1\text{-}KO}$ mice or *Tnfaip3*$^{DNGR1\text{-}KO}$ mice, depicted in pie-chart format, and in (M) higher magnification of bound IgA on *Rag1*^{KO} livers. Results are presented as mean ± SEM of $n = 4$-19 mice per group. *$P < 0.05$, **$P < 0.01$, ****$P < 0.0001$. Scale bars represent 200µm.

3.5. Livers of *Tnfaip3*$^{DNGR1\text{-}KO}$ mice contain increased Tfh-cells and plasma cells, likely producing liver-specific IgA antibodies.

The presence of liver inflammatory lesion with both T-cells and B-cells could indicate direct communication of follicular T-helper (Tfh)-cells with germinal center (GC) B-cells. In *Tnfaip3*$^{DNGR1\text{-}KO}$ mice, the proportions and absolute numbers of Tfh-cells (**Figure 5A/B**) as well as the number GC B-cells and plasma cells (**Figure 5C**) were significantly increased in the livers compared to littermate controls. Moreover, total IgG1 and IgA concentrations were significantly elevated in the serum of 31-week-old *Tnfaip3*$^{DNGR1\text{-}KO}$ mice compared to WT controls (**Figure 5D**). This increase coincided with significantly increased numbers of $IgG1^+$ and IgA^+ plasma cells in spleens and bone marrow (BM) (**Figure 5E/F**). In liver, only IgA^+ plasma cells were significantly increased in *Tnfaip3*$^{DNGR1\text{-}KO}$ mice compared to control mice (**Figure 5G**). Remarkably, we detected increased serum IgG1 and IgA already in 11-week-old mice (**Supplementary Figure 5A**).

We next investigated whether IgG1 and IgA from *Tnfaip3*$^{DNGR1\text{-}KO}$ mice recognised self-antigens, but could not detect significant differences for antibodies against pyruvate dehydrogenase complex subunit E2 (PDC-E2), sp100, glycoprotein 210 (gp210), dsDNA or cardiolipin (**Figure 5H/I/J**). While IgG1 anti-dsDNA and anti-cardiolipin was enhanced in *Tnfaip3*$^{DNGR1\text{-}KO}$ mice compared to WT mice, these concentrations were very low in comparison to the reference serum of lupus-prone *lpr* mice (**Figure 5J**) and most likely not physiological relevant as no IgG deposition nor pathology was observed in the kidneys of *Tnfaip3*$^{DNGR1\text{-}KO}$ mice (**Supplementary Figure 2D/E**).

We next examined whether serum IgG1 or IgA of *Tnfaip3*$^{DNGR1\text{-}KO}$ mice recognized liver-specific proteins. Serum IgG1 from *Tnfaip3*$^{DNGR1\text{-}KO}$ mice did not bind proteins present in liver or pancreas (data not shown). In contrast, serum IgA from 6 out of 10 mice from a panel of 31-week-old *Tnfaip3*$^{DNGR1\text{-}KO}$ mice recognized antigens in the liver periportal regions, while this was only detected by serum IgA from 1 out of 9 WT mice (**Figure 5K/L**). Primarily liver cytoplasmic proteins were recognized by serum IgA from *Tnfaip3*$^{DNGR1\text{-}KO}$ mice (**Figure 5M**). Importantly, serum IgA from 11-week-old *Tnfaip3*$^{DNGR1\text{-}KO}$ mice did not recognize liver-specific proteins, whereas total IgA was elevated at that age

(**Supplementary Figure 5A/B**), indicating that the auto-reactivity of IgA developed after the age of 11 weeks. Serum IgA from ~30% of *Tnfaip3*$^{DNGR1\text{-}KO}$ mice recognized pancreas-specific proteins, albeit with reduced staining intensity compared to liver tissue (**Supplementary figure 5C/D**).

In summary, livers of *Tnfaip3*$^{DNGR1\text{-}KO}$ mice contain increased number of Tfh-cells, GC B-cells, and IgA^{+} plasma cells, accompanied by elevated serum IgG1 and IgA concentrations. Importantly, IgA from *Tnfaip3*$^{DNGR1\text{-}KO}$ mice recognized self-proteins, specifically cytoplasmic proteins of cells within the hepatic periportal regions, which could be involved in the pathogenesis of liver inflammation.

4. DISCUSSION

DCs play a crucial role in the maintenance of tolerance during steady state. The activation status of DCs can act like a switch in the development of tolerance or immunity[6]. Previously we and others have shown that DC-specific ablation of A20/Tnfaip3 led to spontaneous DC activation and subsequently T and B-cell activation, resulting in an inflammatory phenotype resembling SLE[11] or IBD[10]. DCs comprise different subsets and cDCs are primarily known to maintain tolerance[17, 22]. To investigate whether A20/Tnfaip3 deletion in cDCs induces autoimmunity, we crossed *Tnfaip3*-floxed mice to *Clec9a*/DNGR1-cre recombinase mice, as previously this promotor was shown to mainly target cDCs in wild-type mice[27].

In contrast to A20/Tnfaip3 ablation in all DC subsets, which induced systemic autoimmune disease resembling SLE[11] or IBD[10] in mice, *Tnfaip3*$^{DNGR1\text{-}KO}$ mice develop organ-specific autoimmune disease. Aged *Tnfaip3*$^{DNGR1\text{-}KO}$ mice acquired aggravated liver inflammatory infiltrates, consisting mainly of T-cells and some B-cells, adjacent to the portal triads and in lobules. This was accompanied by increased autoreactive IgA in serum, recognizing liver cytoplasmic proteins. DNGR1-driven targeting of DCs in the liver of control mice was similar to other organs[27], being ~95% in cDC1s, ~35% in cDC2s and ~45% in moDCs. However, in *Tnfaip3*$^{DNGR1\text{-}KO}$ mice we found a striking decrease in the proportions of targeted cDC1s (~55%). It is not very likely that the DNGR1-driven excision in cDC1s was reduced in *Tnfaip3*$^{DNGR1\text{-}KO}$ mice. Rather, this finding indicates that due to A20/Tnfaip3-ablation, DC homeostasis was disturbed. Furthermore, liver cDC1s, cDC2s and moDCs show an enhanced activation status (e.g., increased CD40 expression) upon A20/Tnfaip3-ablation.

First signs of chronic liver inflammation, shown by increased cytokeratin 7 expression[37] and liver fibrosis, were found in 24-week-old *Tnfaip3*$^{DNGR1\text{-}KO}$ mice (data not shown) and further increased at 31-weeks of age. Kidneys and intestines, did not show inflammatory lesions, and only very mild inflammation was observed in pancreas. Inflammation plays

an important role in several liver pathologies, and genome-wide association studies (GWAS) have revealed *TNFAIP3* single nucleotide polymorphisms (SNPs) associated to primary biliary cirrhosis (PBC)[38, 39] and autoimmune hepatitis (AIH)[40, 41]. Our data show that A20/Tnfaip3-deletion in cDCs and moDCs leads to spontaneous (auto) immune responses in the liver.

Strikingly, DNGR1-cre mediated deletion of A20/Tnfaip3 in cDC1s reduces the proportion of cells targeted by DNGR1 from ~95% in *Tnfaip3*$^{DNGR1\text{-}WT}$ mice to ~55% in *Tnfaip3*$^{DNGR1\text{-}KO}$ mice. This could be induced by an enhanced sensitivity of cDC1s to undergo apoptosis, which is also regulated by A20/Tnfaip3[42]. As the total number of DNGR1-targeted cDC1s was similar between *Tnfaip3*$^{DNGR1\text{-}WT}$ mice and *Tnfaip3*$^{DNGR1\text{-}KO}$ mice, this suggests that *Tnfaip3*-deficient cDC1s do not undergo apoptosis. The reduced proportion of *Tnfaip3*-deleted cDC1s in *Tnfaip3*$^{DNGR1\text{-}KO}$ mice could be a consequence of a robust selective advantage for the residual *Tnfaip3*-sufficient cDC1s in the *Tnfaip3*$^{DNGR1\text{-}KO}$ mice, as total CD45^{+} hematopoietic cells and thus total DCs increase in the liver. Alternatively, monocytes can adopt to a cDC1-phenotype in the presence of inflammatory signals[43] and start expressing cDC1-typical molecules, like CD103, XCR1, and IRF8. Additional studies are needed to identify the cause for the increase in Tnfaip3-sufficient cDC1s in *Tnfaip3*$^{DNGR1\text{-}KO}$ mice.

Next to DCs, the liver contains other myeloid antigen presenting cells (APCs) such as Kupffer cells and moDCs. Kupffer cell proportions in *Tnfaip3*$^{DNGR1\text{-}KO}$ mice remained constant, while moDCs slightly increased in *Tnfaip3*$^{DNGR1\text{-}KO}$ mice livers, most likely recruited due to liver inflammation[44, 45]. Approximately 30% of moDCs in *Tnfaip3*$^{DNGR1\text{-}KO}$ mice were targeted by DNGR1-driven Cre expression and consequently deleted Tnfaip3. While kidneys are also known to have a similar proportion of DNGR1-Cre-mediated deletion[27], we saw no inflammation in kidneys in *Tnfaip3*$^{DNGR1\text{-}KO}$ mice. Nevertheless, the liver phenotype observed in *Tnfaip3*$^{DNGR1\text{-}KO}$ mice will most likely not be solely induced by Tnfaip3 ablation in cDCs, because affected moDCs may also contribute. Liver cDC1s, cDC2s, and moDCs are activated upon A20/Tnfaip3-ablation, indicated by enhanced co-stimulatory CD40 expression. Subtle differences in CD40 expression on cDCs can lead to substantial differences in T-cell activation, possibly due to a threshold effect. For instance, a 2-fold higher CD40 increase on cDC1s in non-obese diabetic (NOD) mice turns the balance from tolerant Tregs to effector Th1-cell responses[46]. In contrast, absence of CD40 on APCs/DCs during inflammatory conditions expands the number of Tregs[47, 48]. Thus, enhanced CD40 expression on cDCs and a proportion of moDCs in *Tnfaip3*$^{DNGR1\text{-}KO}$ could well explain the increased induction of Th1-cells in the liver. Remarkably, transgenic mice with constitutive CD11c-specific CD40-signalling have a break in tolerance, which coincided with increased Th1 and Th17-cell responses and strikingly also elevated serum IgA[49]. These features are also observed in *Tnfaip3*$^{DNGR1\text{-}KO}$ mice. Evaluating CD40 expression on A20/Tnfaip3-deficient and A20/Tnfaip3-sufficient cDCs within the same *Tnfaip3*$^{DNGR1\text{-}KO}$ mouse

demonstrated that CD40 expression is largely, but not completely regulated by A20/Tnfaip3 in a cell-autonomous way. Suppression of CD40 expression by A20/Tnfaip3 has also been demonstrated in *in vitro* mesothelial cells[50]. However, elevated CD40 expression was also observed on A20/Tnfaip3-sufficient cDCs from *Tnfaip3*$^{DNGR1\text{-}KO}$ mice compared to control mice, suggesting CD40 expression is additionally influenced by cell-extrinsic factors. In *Tnfaip3*$^{DNGR1\text{-}KO}$ mice both cDCs and moDCs expressed higher surface levels of the co-inhibitory molecule PD-L1 which was most likely regulated cell-extrinsically as both A20/Tnfaip3-deficient and A20/Tnfaip3-sufficient cDCs within the same Tnfaip3$^{DNGR1\text{-}KO}$ mouse harbored similar elevated expression compared to control mice. Increased PD-L1 expression is probably driven by enhanced IFNγ[51], produced by liver Th1-cells and CD8$^+$ T-cells (data not shown) in *Tnfaip3*$^{DNGR1\text{-}KO}$ mice.

The inflammatory infiltrates in *Tnfaip3*$^{DNGR1\text{-}KO}$ mouse livers contained CD8$^+$ T-cells, Th-cells, and B-cells. These lymphocytes were detected next to DCs in the periportal inflammatory infiltrates, which could imply local T- and B-cell activation. A number of genes involved in T-cell activation, such as *IL12A*, *IL12RB2* and *STAT4*, all involved in IL-12R signaling, are strongly associated to liver autoimmune biliary diseases[52], and involved in Th1 and Th17-cell polarization. *Tnfaip3*$^{DNGR1\text{-}KO}$ mice showed increased liver Th1-cells and Th17-cells, together with augmented IL-12$^+$ cells, which are present around periportal infiltrates.

Although the percentage of IFNγ-producing CD8$^+$ T-cells did not increase in livers of *Tnfaip3*$^{DNGR1\text{-}KO}$ mice, their total cell number did (data not shown). While the Th1 cytokine IFNγ is hepatotoxic[53] and plays pathological roles in mouse models of autoimmune liver disease[54, 55], controversy exists regarding the function of the Th17 cytokine IL-17A, being either protective[56] or pathogenic[54, 57]. In our study, Th17-cells appeared dispensable for liver inflammation in *Tnfaip3*$^{DNGR1\text{-}KO}$ mice, as the liver pathology was unaltered in the absence of liver IL-17A$^+$ Th-cells (data not shown). Since Th-cell transfer from IFNγ-overexpressing mice induced similar liver pathology[58] as observed in *Tnfaip3*$^{DNGR1\text{-}KO}$ mice, this could be indicative that Th1-cells are pathogenic in *Tnfaip3*$^{DNGR1\text{-}KO}$ mice. Strikingly, the majority of IFNγ-producing Th-cells co-expressed IL-10 in livers from *Tnfaip3*$^{DNGR1\text{-}KO}$ mice, which has broad anti-inflammatory properties. Expression of IL-10 by Th1-cells could be a self-regulatory mechanism to prevent excessive local inflammation[59], as IL-10 can reduce IL-12 secretion from DCs[60].

Aggregation of DCs, T-cells, and B-cells in the livers of *Tnfaip3*$^{DNGR1\text{-}KO}$ mice could promote active TLO formation, in which a GC reaction with help of Tfh-cells would support B-cell activation, class switching, and antibody production. Indeed, liver Tfh-cells, GC B-cells, and plasma cells are increased in *Tnfaip3*$^{DNGR1\text{-}KO}$ mice. In autoimmune liver disease patients, liver Tfh-cells are expanded compared to healthy controls[61] and Tfh-cells even correlate with serum anti-nuclear antibody (ANA) titers[62]. Elevated IgG[63] or IgM[64] are

often seen in autoimmune liver diseases, which are known to correlate with circulating Tfh-cells[65]. The increased liver Tfh-cells in *Tnfaip3*$^{DNGR1\text{-}KO}$ mice may have contributed to establishing elevated serum total IgG and IgA from a young age. In autoimmune liver disease, increased autoreactive IgA is observed[66], which we also find in *Tnfaip3*$^{DNGR1\text{-}KO}$ mice. Serum of *Tnfaip3*$^{DNGR1\text{-}KO}$ mice contained autoreactive IgA specifically recognizing cytoplasmic proteins within the periportal regions. The explicit increase in liver IgA^{+} plasma cells, and not liver IgG1^{+} plasma cells, might explain why only liver-specific autoreactive IgA is observed. As liver periportal inflammation was already present on 11-weeks of age, but autoreactive IgA was not yet detected in *Tnfaip3*$^{DNGR1\text{-}KO}$ mice at that time, this could indicate that auto-antibodies do not initiate liver pathology but rather exacerbate the phenotype.

In summary, DNGR1-cre-mediated deletion of A20/Tnfaip3 in cDCs and moDCs provokes chronic liver inflammatory infiltrates surrounding the portal triads. A20/Tnfaip3 directly controls CD40 expression in liver cDC1s, cDC2s and moDCs *in vivo*, with increased proportions of Th1-cells, Th17-cells, and Tfh-cells and autoreactive B-cell activation. Our data illustrate that activation of conventional DCs and moDCs is sufficient to shift the balance between tolerance and immunity and induces organ-specific autoimmunity, especially in the liver.

Acknowledgements

This project was supported by The Dutch Arthritis Association (12-2-410) and the European Framework program 7 (FP7-MC-CIG grant 304221). We would like to thank Prof. Caetano Reis e Sousa for providing critical mouse strains, Jacobus Hagoort for reviewing the manuscript and Fatemeh Ahmedi and the Erasmus MC Animal Facility (EDC) staff for their assistance during the project.

Conflict of interest

The authors declare no conflict of interest.

REFERENCES

1. Steinman RM. Decisions about dendritic cells: past, present, and future. *Annu Rev Immunol* 2012; 30: 1-22.
2. Hawiger D, Inaba K, Dorsett Y, Guo M, Mahnke K, Rivera M *et al.* Dendritic cells induce peripheral T cell unresponsiveness under steady state conditions in vivo. *J Exp Med* 2001; 194(6): 769-779.
3. Mahnke K, Qian Y, Knop J, Enk AH. Induction of CD4+/CD25+ regulatory T cells by targeting of antigens to immature dendritic cells. *Blood* 2003; 101(12): 4862-4869.
4. Hernandez J, Aung S, Redmond WL, Sherman LA. Phenotypic and functional analysis of CD8(+) T cells undergoing peripheral deletion in response to cross-presentation of self-antigen. *J Exp Med* 2001; 194(6): 707-717.
5. Steinman RM, Hawiger D, Nussenzweig MC. Tolerogenic dendritic cells. *Annu Rev Immunol* 2003; 21: 685-711.
6. Steinman RM, Nussenzweig MC. Avoiding horror autotoxicus: the importance of dendritic cells in peripheral T cell tolerance. *Proc Natl Acad Sci U S A* 2002; 99(1): 351-358.
7. Tan JK, O'Neill HC. Maturation requirements for dendritic cells in T cell stimulation leading to tolerance versus immunity. *J Leukoc Biol* 2005; 78(2): 319-324.
8. Yoshimura S, Bondeson J, Foxwell BM, Brennan FM, Feldmann M. Effective antigen presentation by dendritic cells is NF-kappaB dependent: coordinate regulation of MHC, co-stimulatory molecules and cytokines. *International immunology* 2001; 13(5): 675-683.
9. Wertz IE, O'Rourke KM, Zhou H, Eby M, Aravind L, Seshagiri S *et al.* De-ubiquitination and ubiquitin ligase domains of A20 downregulate NF-kappaB signalling. *Nature* 2004; 430(7000): 694-699.
10. Hammer GE, Turer EE, Taylor KE, Fang CJ, Advincula R, Oshima S *et al.* Expression of A20 by dendritic cells preserves immune homeostasis and prevents colitis and spondyloarthritis. *Nat Immunol* 2011; 12(12): 1184-1193.
11. Kool M, van Loo G, Waelput W, De Prijck S, Muskens F, Sze M *et al.* The ubiquitin-editing protein A20 prevents dendritic cell activation, recognition of apoptotic cells, and systemic autoimmunity. *Immunity* 2011; 35(1): 82-96.
12. Ma A, Malynn BA. A20: linking a complex regulator of ubiquitylation to immunity and human disease. *Nat Rev Immunol* 2012; 12(11): 774-785.
13. Das T, Chen Z, Hendriks RW, Kool M. A20/Tumor Necrosis Factor alpha-Induced Protein 3 in Immune Cells Controls Development of Autoinflammation and Autoimmunity: Lessons from Mouse Models. *Front Immunol* 2018; 9: 104.
14. Coombes JL, Siddiqui KR, Arancibia-Carcamo CV, Hall J, Sun CM, Belkaid Y *et al.* A functionally specialized population of mucosal CD103+ DCs induces Foxp3+ regulatory T cells via a TGF-beta and retinoic acid-dependent mechanism. *J Exp Med* 2007; 204(8): 1757-1764.
15. Khare A, Krishnamoorthy N, Oriss TB, Fei M, Ray P, Ray A. Cutting edge: inhaled antigen upregulates retinaldehyde dehydrogenase in lung CD103+ but not plasmacytoid dendritic cells to induce Foxp3 de novo in CD4+ T cells and promote airway tolerance. *J Immunol* 2013; 191(1): 25-29.
16. Yamazaki S, Dudziak D, Heidkamp GF, Fiorese C, Bonito AJ, Inaba K *et al.* CD8+ CD205+ splenic dendritic cells are specialized to induce Foxp3+ regulatory T cells. *J Immunol* 2008; 181(10): 6923-6933.
17. Bonifaz L, Bonnyay D, Mahnke K, Rivera M, Nussenzweig MC, Steinman RM. Efficient targeting of protein antigen to the dendritic cell receptor DEC-205 in the steady state leads to antigen presentation on

major histocompatibility complex class I products and peripheral CD8+ T cell tolerance. *J Exp Med* 2002; 196(12): 1627-1638.

18. Luckashenak N, Schroeder S, Endt K, Schmidt D, Mahnke K, Bachmann MF *et al.* Constitutive crosspresentation of tissue antigens by dendritic cells controls CD8+ T cell tolerance in vivo. *Immunity* 2008; 28(4): 521-532.
19. Hildner K, Edelson BT, Purtha WE, Diamond M, Matsushita H, Kohyama M *et al.* Batf3 deficiency reveals a critical role for CD8alpha+ dendritic cells in cytotoxic T cell immunity. *Science* 2008; 322(5904): 1097-1100.
20. Edelson BT, Kc W, Juang R, Kohyama M, Benoit LA, Klekotka PA *et al.* Peripheral CD103+ dendritic cells form a unified subset developmentally related to CD8alpha+ conventional dendritic cells. *J Exp Med* 2010; 207(4): 823-836.
21. Luda KM, Joeris T, Persson EK, Rivollier A, Demiri M, Sitnik KM *et al.* IRF8 Transcription-Factor-Dependent Classical Dendritic Cells Are Essential for Intestinal T Cell Homeostasis. *Immunity* 2016; 44(4): 860-874.
22. Dudziak D, Kamphorst AO, Heidkamp GF, Buchholz VR, Trumpfheller C, Yamazaki S *et al.* Differential antigen processing by dendritic cell subsets in vivo. *Science* 2007; 315(5808): 107-111.
23. Guilliams M, Crozat K, Henri S, Tamoutounour S, Grenot P, Devilard E *et al.* Skin-draining lymph nodes contain dermis-derived CD103(-) dendritic cells that constitutively produce retinoic acid and induce Foxp3(+) regulatory T cells. *Blood* 2010; 115(10): 1958-1968.
24. Plantinga M, Guilliams M, Vanheerswynghels M, Deswarte K, Branco-Madeira F, Toussaint W *et al.* Conventional and monocyte-derived CD11b(+) dendritic cells initiate and maintain T helper 2 cell-mediated immunity to house dust mite allergen. *Immunity* 2013; 38(2): 322-335.
25. Schlitzer A, McGovern N, Teo P, Zelante T, Atarashi K, Low D *et al.* IRF4 transcription factor-dependent CD11b+ dendritic cells in human and mouse control mucosal IL-17 cytokine responses. *Immunity* 2013; 38(5): 970-983.
26. Randolph GJ, Inaba K, Robbiani DF, Steinman RM, Muller WA. Differentiation of phagocytic monocytes into lymph node dendritic cells in vivo. *Immunity* 1999; 11(6): 753-761.
27. Schraml BU, van Blijswijk J, Zelenay S, Whitney PG, Filby A, Acton SE *et al.* Genetic tracing via DNGR-1 expression history defines dendritic cells as a hematopoietic lineage. *Cell* 2013; 154(4): 843-858.
28. Vereecke L, Sze M, Mc Guire C, Rogiers B, Chu Y, Schmidt-Supprian M *et al.* Enterocyte-specific A20 deficiency sensitizes to tumor necrosis factor-induced toxicity and experimental colitis. *J Exp Med* 2010; 207(7): 1513-1523.
29. Srinivas S, Watanabe T, Lin CS, William CM, Tanabe Y, Jessell TM *et al.* Cre reporter strains produced by targeted insertion of EYFP and ECFP into the ROSA26 locus. *BMC Dev Biol* 2001; 1: 4.
30. van de Garde MD, Movita D, van der Heide M, Herschke F, De Jonghe S, Gama L *et al.* Liver Monocytes and Kupffer Cells Remain Transcriptionally Distinct during Chronic Viral Infection. *PLoS One* 2016; 11(11): e0166094.
31. Vroman H, Bergen IM, Li BW, van Hulst JA, Lukkes M, van Uden D *et al.* Development of eosinophilic inflammation is independent of B-T cell interaction in a chronic house dust mite-driven asthma model. *Clin Exp Allergy* 2017; 47(4): 551-564.
32. Marlow SL, Blennerhassett MG. Deficient innervation characterizes intestinal strictures in a rat model of colitis. *Exp Mol Pathol* 2006; 80(1): 54-66.
33. Ishak K, Baptista A, Bianchi L, Callea F, De Groote J, Gudat F *et al.* Histological grading

and staging of chronic hepatitis. *Journal of hepatology* 1995; 22(6): 696-699.

34. Yang CY, Leung PS, Yang GX, Kenny TP, Zhang W, Coppel R *et al.* Epitope-specific anti-nuclear antibodies are expressed in a mouse model of primary biliary cirrhosis and are cytokine-dependent. *Clin Exp Immunol* 2012; 168(3): 261-267.
35. Mombaerts P, Iacomini J, Johnson RS, Herrup K, Tonegawa S, Papaioannou VE. RAG-1-deficient mice have no mature B and T lymphocytes. *Cell* 1992; 68(5): 869-877.
36. Washington MK. Autoimmune liver disease: overlap and outliers. *Mod Pathol* 2007; 20 Suppl 1: S15-30.
37. Bateman AC, Hubscher SG. Cytokeratin expression as an aid to diagnosis in medical liver biopsies. *Histopathology* 2010; 56(4): 415-425.
38. Cordell HJ, Han Y, Mells GF, Li Y, Hirschfield GM, Greene CS *et al.* International genome-wide meta-analysis identifies new primary biliary cirrhosis risk loci and targetable pathogenic pathways. *Nat Commun* 2015; 6: 8019.
39. Juran BD, Hirschfield GM, Invernizzi P, Atkinson EJ, Li Y, Xie G *et al.* Immunochip analyses identify a novel risk locus for primary biliary cirrhosis at 13q14, multiple independent associations at four established risk loci and epistasis between 1p31 and 7q32 risk variants. *Human molecular genetics* 2012; 21(23): 5209-5221.
40. de Boer YS, van Gerven NM, Zwiers A, Verwer BJ, van Hoek B, van Erpecum KJ *et al.* Genome-wide association study identifies variants associated with autoimmune hepatitis type 1. *Gastroenterology* 2014; 147(2): 443-452 e445.
41. Xu E, Cao H, Lin L, Liu H. rs10499194 polymorphism in the tumor necrosis factor-alpha inducible protein 3 (TNFAIP3) gene is associated with type-1 autoimmune hepatitis risk in Chinese Han population. *PLoS One* 2017; 12(4): e0176471.
42. Onizawa M, Oshima S, Schulze-Topphoff U, Oses-Prieto JA, Lu T, Tavares R *et al.* The ubiquitin-modifying enzyme A20 restricts ubiquitination of the kinase RIPK3 and protects cells from necroptosis. *Nat Immunol* 2015; 16(6): 618-627.
43. Sharma MD, Rodriguez PC, Koehn BH, Baban B, Cui Y, Guo G *et al.* Activation of p53 in Immature Myeloid Precursor Cells Controls Differentiation into Ly6c(+)CD103(+) Monocytic Antigen-Presenting Cells in Tumors. *Immunity* 2018; 48(1): 91-106.
44. Dominguez PM, Ardavin C. Differentiation and function of mouse monocyte-derived dendritic cells in steady state and inflammation. *Immunol Rev* 2010; 234(1): 90-104.
45. Sutti S, Locatelli I, Bruzzi S, Jindal A, Vacchiano M, Bozzola C *et al.* CX3CR1-expressing inflammatory dendritic cells contribute to the progression of steatohepatitis. *Clinical science (London, England : 1979)* 2015; 129(9): 797-808.
46. Price JD, Beauchamp NM, Rahir G, Zhao Y, Rieger CC, Lau-Kilby AW *et al.* CD8+ dendritic cell-mediated tolerance of autoreactive CD4+ T cells is deficient in NOD mice and can be corrected by blocking CD40L. *J Leukoc Biol* 2014; 95(2): 325-336.
47. Richer MJ, Lavallee DJ, Shanina I, Horwitz MS. Immunomodulation of antigen presenting cells promotes natural regulatory T cells that prevent autoimmune diabetes in NOD mice. *PLoS One* 2012; 7(2): 15.
48. Zheng X, Suzuki M, Ichim TE, Zhang X, Sun H, Zhu F *et al.* Treatment of autoimmune arthritis using RNA interference-modulated dendritic cells. *J Immunol* 2010; 184(11): 6457-6464.
49. Barthels C, Ogrinc A, Steyer V, Meier S, Simon F, Wimmer M *et al.* CD40-signalling abrogates induction of RORgammat(+) Treg cells by intestinal CD103(+) DCs and causes fatal colitis. *Nat Commun* 2017; 8: 14715.
50. Zou XL, Pei DA, Yan JZ, Xu G, Wu P. A20 overexpression inhibits lipopolysaccha-

ride-induced NF-kappaB activation, TRAF6 and CD40 expression in rat peritoneal mesothelial cells. *Int J Mol Sci* 2014; 15(4): 6592-6608.

51. Freeman GJ, Long AJ, Iwai Y, Bourque K, Chernova T, Nishimura H *et al.* Engagement of the PD-1 immunoinhibitory receptor by a novel B7 family member leads to negative regulation of lymphocyte activation. *J Exp Med* 2000; 192(7): 1027-1034.
52. Webb GJ, Siminovitch KA, Hirschfield GM. The immunogenetics of primary biliary cirrhosis: A comprehensive review. *J Autoimmun* 2015; 64: 42-52.
53. Kano A, Watanabe Y, Takeda N, Aizawa S, Akaike T. Analysis of IFN-gamma-induced cell cycle arrest and cell death in hepatocytes. *J Biochem* 1997; 121(4): 677-683.
54. Kawata K, Tsuda M, Yang GX, Zhang W, Tanaka H, Tsuneyama K *et al.* Identification of potential cytokine pathways for therapeutic intervention in murine primary biliary cirrhosis. *PLoS One* 2013; 8(9): e74225.
55. Toyonaga T, Hino O, Sugai S, Wakasugi S, Abe K, Shichiri M *et al.* Chronic active hepatitis in transgenic mice expressing interferon-gamma in the liver. *Proc Natl Acad Sci U S A* 1994; 91(2): 614-618.
56. Yang W, Yao Y, Yang YQ, Lu FT, Li L, Wang YH *et al.* Differential modulation by IL-17A of Cholangitis versus Colitis in IL-2Ralpha deleted mice. *PLoS One* 2014; 9(8): e105351.
57. Yu H, Huang J, Liu Y, Ai G, Yan W, Wang X *et al.* IL-17 contributes to autoimmune hepatitis. *J Huazhong Univ Sci Technolog Med Sci* 2010; 30(4): 443-446.
58. Bae HR, Leung PS, Tsuneyama K, Valencia JC, Hodge DL, Kim S *et al.* Chronic expression of interferon-gamma leads to murine autoimmune cholangitis with a female predominance. *Hepatology* 2016; 64(4): 1189-1201.
59. Jankovic D, Kullberg MC, Feng CG, Goldszmid RS, Collazo CM, Wilson M *et al.* Conventional T-bet(+)Foxp3(-) Th1 cells are the major source of host-protective regulatory IL-10 during intracellular protozoan infection. *J Exp Med* 2007; 204(2): 273-283.
60. De Smedt T, Van Mechelen M, De Becker G, Urbain J, Leo O, Moser M. Effect of interleukin-10 on dendritic cell maturation and function. *European journal of immunology* 1997; 27(5): 1229-1235.
61. Wang L, Sun Y, Zhang Z, Jia Y, Zou Z, Ding J *et al.* CXCR5+ CD4+ T follicular helper cells participate in the pathogenesis of primary biliary cirrhosis. *Hepatology* 2015; 61(2): 627-638.
62. Kimura N, Yamagiwa S, Sugano T, Setsu T, Tominaga K, Kamimura H *et al.* Possible involvement of chemokine C-C receptor 7(-) programmed cell death-1(+) follicular helper T-cell subset in the pathogenesis of autoimmune hepatitis. *Journal of gastroenterology and hepatology* 2018; 33(1): 298-306.
63. Hennes EM, Zeniya M, Czaja AJ, Pares A, Dalekos GN, Krawitt EL *et al.* Simplified criteria for the diagnosis of autoimmune hepatitis. *Hepatology* 2008; 48(1): 169-176.
64. Taal BG, Schalm SW, de Bruyn AM, de Rooy FW, Klein F. Serum IgM in primary biliary cirrhosis. *Clinica chimica acta; international journal of clinical chemistry* 1980; 108(3): 457-463.
65. Ma L, Qin J, Ji H, Zhao P, Jiang Y. Tfh and plasma cells are correlated with hypergammaglobulinaemia in patients with autoimmune hepatitis. *Liver Int* 2014; 34(3): 405-415.
66. Nishio A, Van de Water J, Leung PS, Joplin R, Neuberger JM, Lake J *et al.* Comparative studies of antimitochondrial autoantibodies in sera and bile in primary biliary cirrhosis. *Hepatology* 1997; 25(5): 1085-1089.

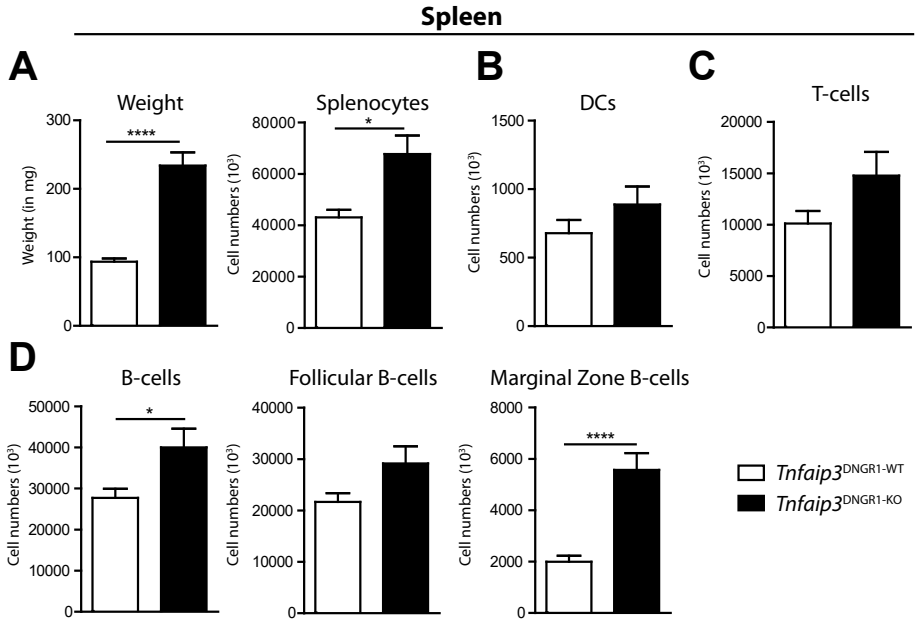

Supplementary Figure 1: *Tnfaip3*$^{DNGR1\text{-}KO}$ mice have splenomegaly with increased marginal zone B-cells.

Tnfaip3$^{DNGR1\text{-}WT}$ mice and *Tnfaip3*$^{DNGR1\text{-}KO}$ mice were analyzed at 31-weeks of age. (**A**) Quantification of both spleen weight and total cell count. (**B-C**) Enumeration of dendritic cells (CD11c^{hi}MHC-II^{hi}) (**B**) T-cells (CD3^{+}) (**C**), B-cells (CD19^{+}B220^{+}), Follicular B-cells (CD19^{+}B220^{+}CD23^{+}) and marginal zone B-cells (CD19^{+}B220^{+}CD21/35^{+}) (**D**) in spleen cell suspensions by flow cytometry. Results are presented as mean ± SEM and is pooled data from 3 independent experiments, n = 9-15 per group. *$P < 0.05$, ****$P < 0.0001$.

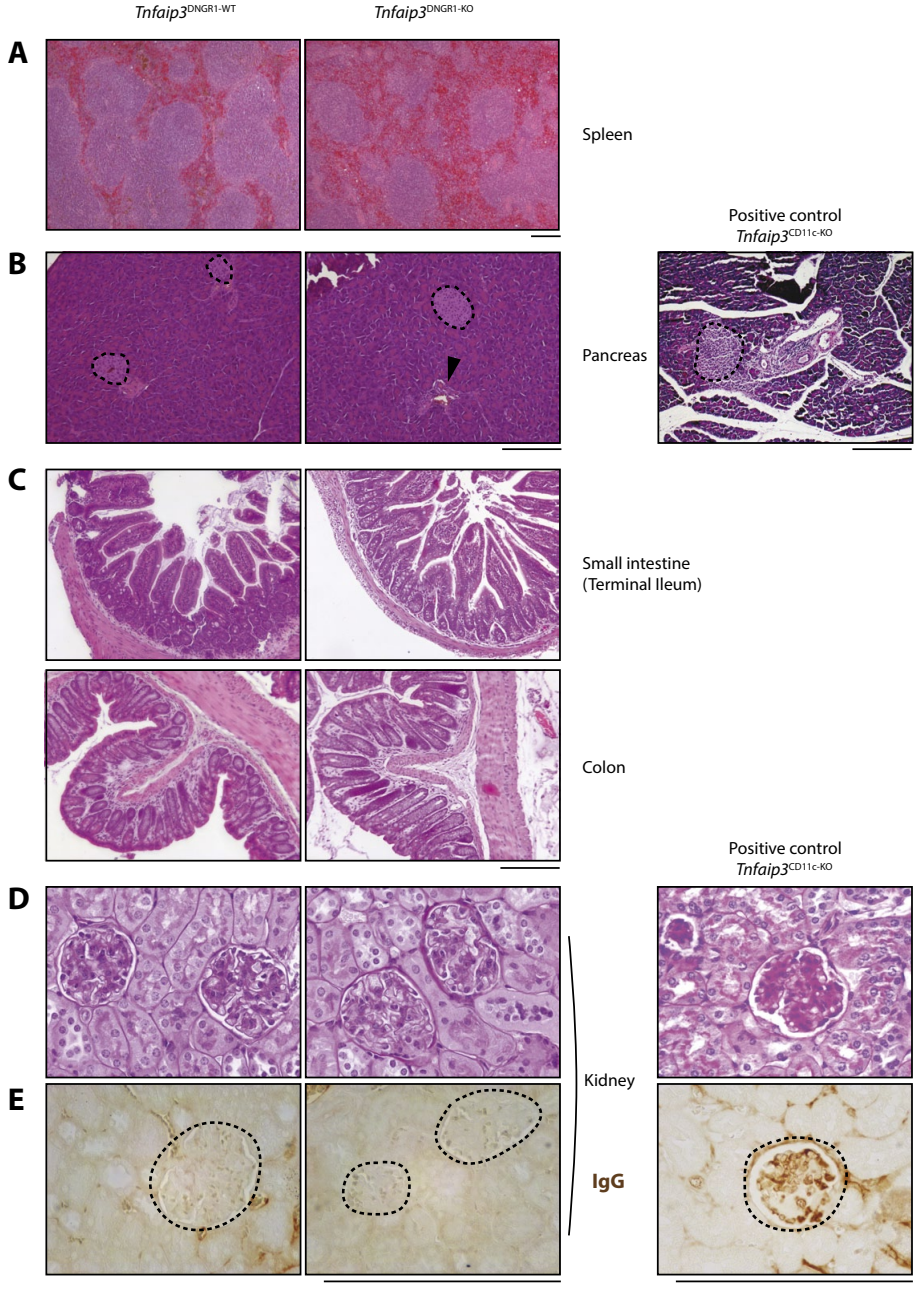

Supplementary Figure 2: Most tissues have absence of inflammation in *Tnfaip3*$^{DNGR1\text{-}KO}$ mice.
(**A-C**) H&E staining of spleens (**A**), pancreas (**B**) and terminal ileum and colon (**C**) from 31-week-old *Tnfaip3*$^{DNGR1\text{-}KO}$ mice. Arrowheads indicate mild inflammatory infiltrate. (**D**) Periodic acid-Schiff (PAS)$^{+}$ staining of kidneys from 31-week-old *Tnfaip3*$^{DNGR1\text{-}WT}$ mice and *Tnfaip3*$^{DNGR1\text{-}KO}$ mice. (**E**) Immunohistochemistry for glomerular IgG^{+} (brown) depositions in kidneys of 31-week-old mice. Dashed line highlights glomeruli. A lupus mouse positive control (*Cd11c*-cre mediated *Tnfaip3*-deleted mice) is also illustrated for comparison. Scale bars represent 200µm.

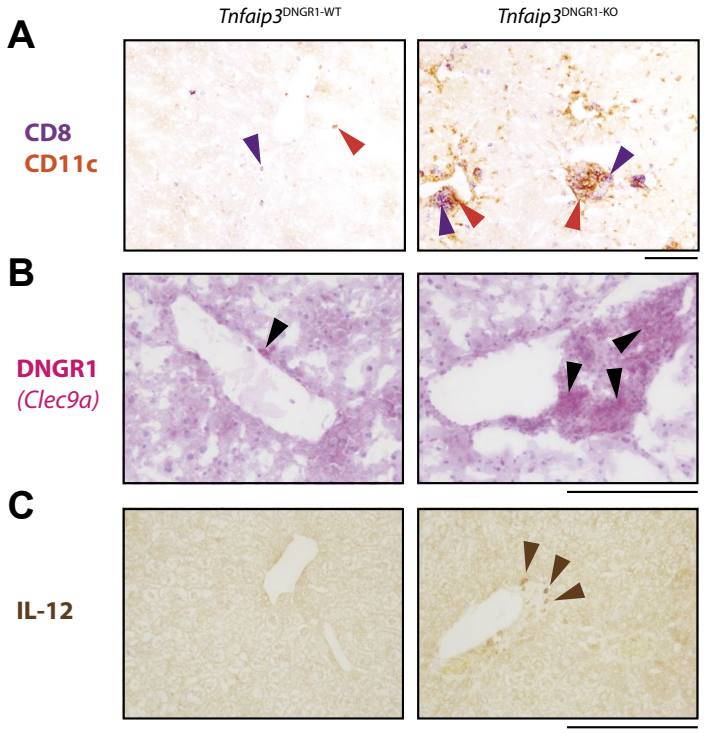

Supplementary Figure 3: Inflammatory infiltrates in *Tnfaip3*$^{DNGR1-KO}$ mice contain DCs, CD8$^+$ T-cells and DNGR1$^+$ cells.
(**A-C**) Immunohistochemistry for CD8$^+$ (purple, arrowhead) and CD11c$^+$ cells (orange, arrowhead) (**A**) DNGR1$^+$ cells (pink, arrowhead, positive in n=5/5 mice) (**B**) and IL-12 (brown, arrowhead, positive in n=4/6 mice) (**C**) in livers of 31-week-old *Tnfaip3*$^{DNGR1-WT}$ mice and *Tnfaip3*$^{DNGR1-KO}$ mice. Scale bars represent 200µm.

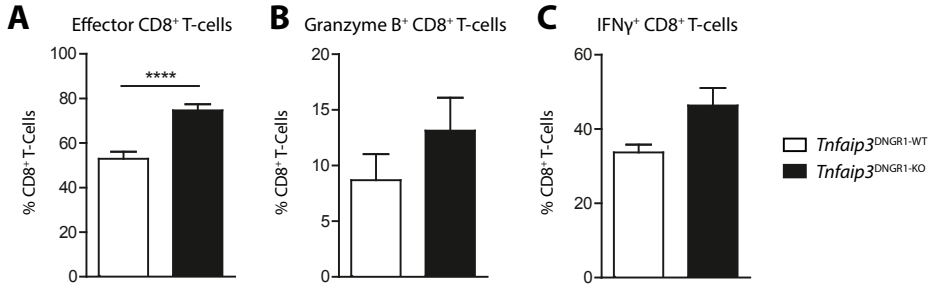

Supplementary Figure 4: *Tnfaip3*$^{DNGR1-KO}$ mice have increased liver CD8$^+$ T-cell activation.
Tnfaip3$^{DNGR1-WT}$ mice and *Tnfaip3*$^{DNGR1-KO}$ mice were sacrificed at 31-weeks of age under naïve conditions and the livers were examined. (**A-C**) Quantification of the proportion activated (CD44$^+$) (**A**), Granzyme B$^+$ (**B**) and IFNγ$^+$ (**C**) CD8$^+$ T-cells using flow cytometry. Pooled data from 4 experiments is shown for (**A**), 3 experiments for (**B**) and representative data from one out of 2 experiment is shown for (**C**). Results are presented as mean ± SEM of n = 4-19 per group. ****P < 0.0001.

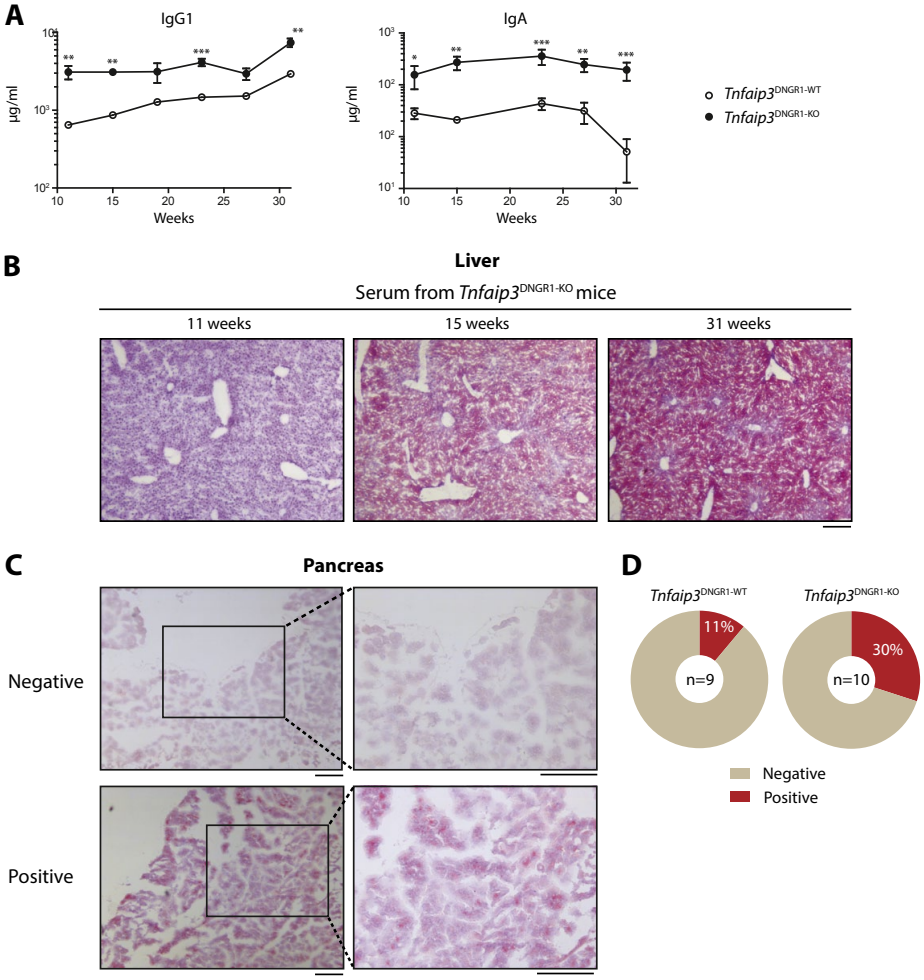

Supplementary Figure 5: IgA from *Tnfaip3*$^{DNGR1-KO}$ mice are primarily directed to liver antigens.
Serum of *Tnfaip3*$^{DNGR1-WT}$ mice and *Tnfaip3*$^{DNGR1-KO}$ mice was obtained. (**A**) Quantification of IgG1 and IgA immunoglobulin levels over time between 11 and 31-week-old mice. (**B**) Representative illustration of IgA autoreactivity towards liver proteins on liver of *Rag1*^{KO} mice in serum of 11, 15 and 31-week-old *Tnfaip-3*$^{DNGR1-KO}$ mice. (**C-D**) Representative negative and positive IgA staining on pancreas of *Rag1*^{KO} mice (**C**) and illustrated in pie chart format from both *Tnfaip3*$^{DNGR1-WT}$ mice and *Tnfaip3*$^{DNGR1-KO}$ mice (**D**). Results are from 2 experiments presented as mean ± SEM of n = 6-10 per group. *P<0.05, **P < 0.01, ***P < 0.001. Scale bars represent 200µm.

SUPPLEMENTARY MATERIAL METHODS:

Liver and Kidney (immuno)histochemistry

Liver cryosections were stained for DNGR1 (*Clec9a*, included in **Supplementary table 2**) and CD11c with CD8 (also included in **Supplementary table 2**). Cryo-sections were initially fixed in acetone. Sections were then incubated for 1hr with the primary antibodies. After washing, slides were incubated for 30 min with secondary antibodies (**Supplementary table 2**). Diaminobenzene (DAB) (for CD11c), Fast blue alkaline phosphatase (for CD8) and new fuchsin alkaline phosphatase (for DNGR1) substrates were used to retrieve specific staining. Counterstaining was performed with Gills hematoxylin (Sigma) (only for DNGR1-staining).

Six-µm-thick paraffin embedded kidney sections were stained with Periodic Acid Schiff (PAS; Sigma). For immunohistochemical stainings, antigen retrieval on paraffin-sections were established using citrate buffer (Sigma Aldrich). Paraffin kidney sections were stained for IgG with the primary antibody (**Supplementary table 2**) and paraffin liver sections were stained for IL-12 (**Supplementary table 2**). After washing, slides were incubated for 30 min with secondary antibodies (**Supplementary table 2**). The anti-Rabbit ABC Peroxidase Kit was utilized (Vector Labs, Burlingame, CA, USA). Diaminobenzene (DAB) was used to retrieve specific staining.

Supplementary Table 1: Antibodies used for flow cytometry.

Antibody	Conjugate	Clone	Company
B220	Alexa Fluor 700	RA3-6B2	eBioscience
B220	Pe-Cy7	RA3-6B2	eBioscience
CD103	ef450	2E7	eBioscience
CD11b	Biotin	M1/70	BD
CD11c	PE-Texas Red	N418	Invitrogen
CD138	Brilliant Violet 605	281-2	BD
CD19	APC-Cy7	1D3	BD
CD25	Biotin	PC61.5	eBioscience
CD3	PE-CF594	145-2C11	BD
CD4	Brilliant Violet 605	RM4-5	BD
CD4	Brilliant Violet 711	RM4-5	BD
CD44	FITC	IM7	eBioscience
CD44	APC-Cy7	IM7	BD
CD45	Brilliant Violet 711	30-F11	BD
CD45	PerCP-ef710	30-F11	eBioscience
CD62L	APC-ef780	MEL-14	eBioscience
CD64	Alexa Fluor 647	X54-5/7.1	BD
CD8	PE-Cy7	53-6.7	eBioscience
CD95	PE-Texas Red	Jo2	BD
CXCR5	Biotin	J43	eBioscience
F4/80	APC-ef780	BM8	eBioscience
FCεRIα	Biotin	MAR-1	eBioscience
Foxp3	Alexa Fluor 700	FJK-16s	eBioscience
Granzyme B	PE	MHGB04	Caltag
IFN-γ	ef450	XMG1.2	eBioscience
IgA	FITC	C10-3	BD
IgD	APC	11-26c	eBiosicence
IgG1	PE	A85-1	BD
IgM	PE-Cy7	II/41	eBioscience
IL-10	Alexa Fluor 488	JES5-16E3	eBioscience
IL-17A	Alexa Fluor 700	TC11-18H10.1	BD
Ly6G/GR1	FITC	RB6.8C5	eBioscience
MHC-II	Alexa Fluor 700	M5/114.15.3	eBioscience
NK1.1	PE	PK136	eBioscience
PD1	Brilliant Violet 421	J43	BD
RORγt	PerCP-Cy5.5	Q31-378	BD
Streptavidin	Brilliant Violet 786		BD
Streptavidin	Brilliant Violet 711		BD

Supplementary Table 2: Primary and secondary antibodies for Immunohistochemistry

Primary Antibody	Clone	Company	Secondary Antibody	Product code	Company
Rat anti-CD8-PE	53-6.7	eBioscience, San Diego, CA, USA	**Goat anti-R-phycoerythrin AP**	600-105-387	Rockland, Limerick, PA, USA
Hamster anti-CD11c	N418	eBioscience, San Diego, CA, USA	**Goat anti-Hamster PO**	127-035-099	Jackson Immunoresearch, West Grove, PA, USA
Rabbit anti-Cytokeratin 7	EPR17078	Abcam, Cambridge,UK	**Goat anti-Rabbit PO**	PK-4001	Vector Laboratories, Burlingame, CA, USA
Rat anti-CLEC9a	MAB67761	R&D, Minneapolis, MN, USA	**Goat anti-RAT AP**	112-055-167	Jackson Immunoresearch
Rabbit anti-CD3	Polyclonal	DAKO, Glostrup, Denmark	**Goat anti-Rabbit PO**	PK-4001	Vector Laboratories
Rat anti-B220	RA3-6B2	Bioceros, Utrecht, The Netherlands	**Goat anti-RAT AP**	112-055-167	Jackson Immunoresearch
Goat anti-IgG-Biotin		Southern Biotech, Birmingham, AL, USA	**VECTASTAIN® ABC-HRP Kit**	PK-6100	Vector Laboratories, Burlingame, CA, USA
Rabbit anti-IL-12	EP5737	Abcam, Cambridge,UK	**Goat anti-Rabbit PO**	PK-4001	Vector Laboratories, Burlingame, CA, USA